Title: Ultrasound Computed Tomography for Imaging Tissue-Engineered Blood Vessel

by

Enxhi Jaupi

A Thesis

Submitted to the Faculty

of the

WORCESTER POLYTECHNIC INSTITUTE

In partial fulfillment of the requirements for the

Degree of Master of Science

in
Biomedical Engineering

by

_____

May 2022

APPROVED:

_____
Professor Haichong K. Zhang, Primary Thesis Advisor

_____
Professor Karen Troy, Committee Member

_____
Professor Marsha Rolle, Committee Member

_____
Professor Loris Fichera, Committee Member

Abstract

Tissue-engineered blood vessel (TEBV) technologies have made it possible to develop model systems to study cardiovascular disease pathology and discover new treatments. However, fabricating a TEBV is a complex process. A fully grown tissue typically needs several weeks to fabricate, and tissue development depends on several factors, including cell source and chemical and mechanical stimulation. Current evaluation tools like histology and scanning electron microscopy allow us to measure the geometry of the tissue but are destructive. Therefore, a new, non-destructive evaluation tool is needed to perform serial geometry measurements of the TEBV to monitor tissue development and remodeling. We proposed an ultrasound computer tomography (USCT) imaging system that provides an alternative way to achieve non-invasive TEBV growth monitoring. The USCT system consists of a single-element transducer that moves in a circular trajectory along the bioreactor and collects A-lines of the cross-section of the TEBV. A back-projection algorithm is used to reconstruct the image from acquired A-lines. First, we used a needle phantom to evaluate the point spread function (PSF) to validate the system. After the system was validated, TEBV was imaged. Next, we used histology to validate the dimensions of the TEBV obtained from the image. From the scanned image, we successfully visualized the cross-section of the TEBV. In addition, from the cross-section of the TEBV, we can measure the dimension of the tissue wall. Following USCT imaging, the TEBV was processed for histology and hematoxylin and eosin (H&E) staining to measure TEBV wall thickness. Last, we compare the dimension tissue wall of the plot and the histology. The results demonstrated USCT imaging system could be an evaluating tool to provide serial, non-destructive geometry measurements of the TEBV during culture.

Keywords used: "Imaging Tissue Engineering; Imaging Techniques in Tissue Engineering; Ultrasound Computer Tomography Imaging; Tissue-Engineered Blood Vessel.

ACKNOWLEDGMENTS

This project was a collaboration between Medical FUSION Laboratory and Rolle Laboratory. Financial support was provided by Worcester Polytechnic Institute (WPI) Internal Fund. Bioreactor prototypes were designed and constructed at the Politecnico di Milano in Milan, Italy (Piola, M., Fiore, G. B., Soncini, M) and provided to the Rolle Lab.

First, I want to thank my professor advisor, Ph.D. Haichong Zhang for his teaching and continued support during these two years of my master's program. Second, I want to thank Professor Marsha Rolle, Yichuan Tang, Shang Gao, William DeMaria, and Andre Figueroa for their help and support. Third, I want to thank you, colleagues from the Medical Fusion Laboratory, and the Fulbright community for allowing me to be part of this project.

Contents

List of Figures

List of Tables

1. Tissue-engineered blood vessel (TEBV)

1.1 Introduction to TEBV

Tissue engineering is a novel field that applies the principle of engineering and life sciences to restore damaged tissue function and structure using in vitro artificially created ones. Tissue-engineered blood vessel (TEBV) cultivation technologies were first developed in the 1980s. They were constructed as synthetic grafts and used as an alternative treatment for blood vessel defects caused by various cardiovascular diseases or traumatic injuries [3].

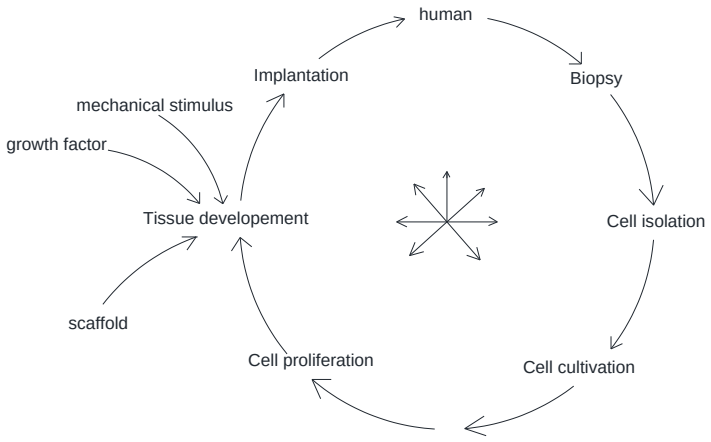

Figure 1. The schematic diagram of the tissue engineering steps [1].

Nowadays, new treatments for cardiovascular diseases are tested in animal models and 2D cell cultures. However, 2D cultures do not represent the 3D mechanical environment [3]. Furthermore, cell-matrix interactions found in vivo and animal studies do not accurately predict the success of drugs in humans; many successful drugs in animals fail in human clinical trials. Thus, there is a need for 3D human tissues to model cardiovascular diseases and serve as tools to screen potential therapies [3]. In addition, testing drugs on functional human tissues in vitro may allow researchers to eliminate ineffective drugs in the testing process and accelerate the development of new treatments [3]. A novel approach for this issue is fabricating functional 3D human vascular tissue from human cells for drug screening and disease modeling.

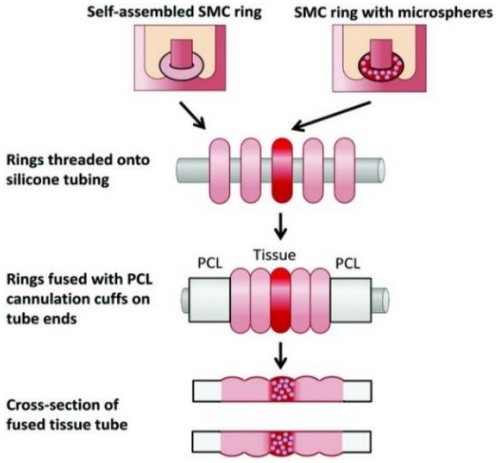

Figure 2. The fabrication of modular tissue tubes with focal heterogeneities. The resulting construct is a fused tissue tube with a focal region of microsphere incorporation. [3] Reproduced with permission [3].

One example is fabricating functional human tissue-engineered blood vessels (TEBVs) to model vascular diseases, such as aneurysms and intimal hyperplasia. Tissue engineering has made it possible to develop model systems to study vascular disease pathology and discover new drugs or treatment options for patients. Most vascular diseases clinically present as focal lesions within a patient's blood vessel wall [3]. Although there has been significant research on constructing and using Tissue-engineered blood vessels, a non-destructive method to monitor their growth and vitality inside the bioreactor during development and culture is still a problem to be solved. Conventionally, to examine the quality of the tissue cultivated inside, a bioreactor needs to be opened to access the tissue. A non-destructive method for monitoring the growth of Tissue-engineered blood vessels could help optimize the growing procedure. Time and funds can be saved by detecting which vessel will not be cultivated successfully.

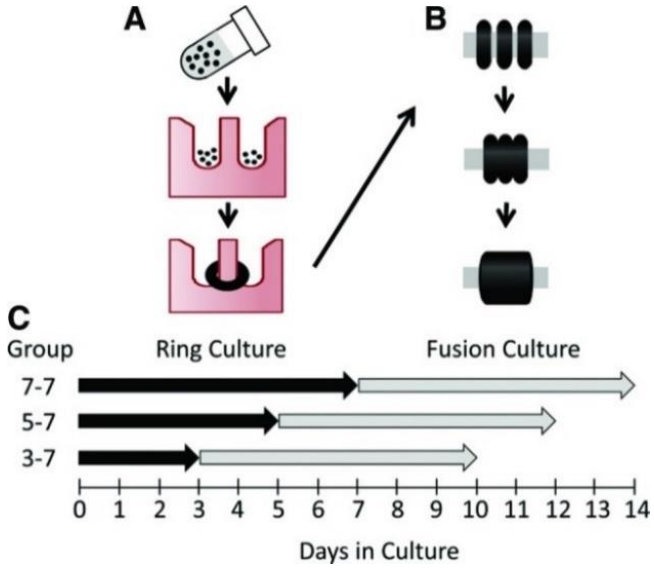

Figure 3. The schematic of the tube fabrication process and tissue tube culture experimental groups. [3] Reproduced with permission [3].

In addition, when there is a need to evaluate different cultivation methods, such non-invasive monitoring could provide data through the cultivation process. For example, engineered tissue needs a three-dimensional and time-lapse in vivo analysis to analyze its geometrics parameters and the quality of the tissue pre-construction and after. Furthermore, such in-process data could contribute to the optimization of specific cultivation methods to improve efficiency [3].

1.2 Bioreactor

The bioreactor is an apparatus for growing organisms, bacteria, yeast, or animal cells under controlled conditions. The bioreactor is designed based on the biological reaction that carries out—an example of a bioreactor used to culture cells for cellular immobilization. The type of bioreactor used in this work is the luminal flow with a pressure loop shown in image 3. This bioreactor is used to fabricate TEBV, but the goal is to fabricate model diseased TEBV. Fabrication of a fully grown tissue from a luminal flow bioreactor typically needs several weeks, and tissue development depends on several factors, including cell source and chemical and mechanical stimulation.

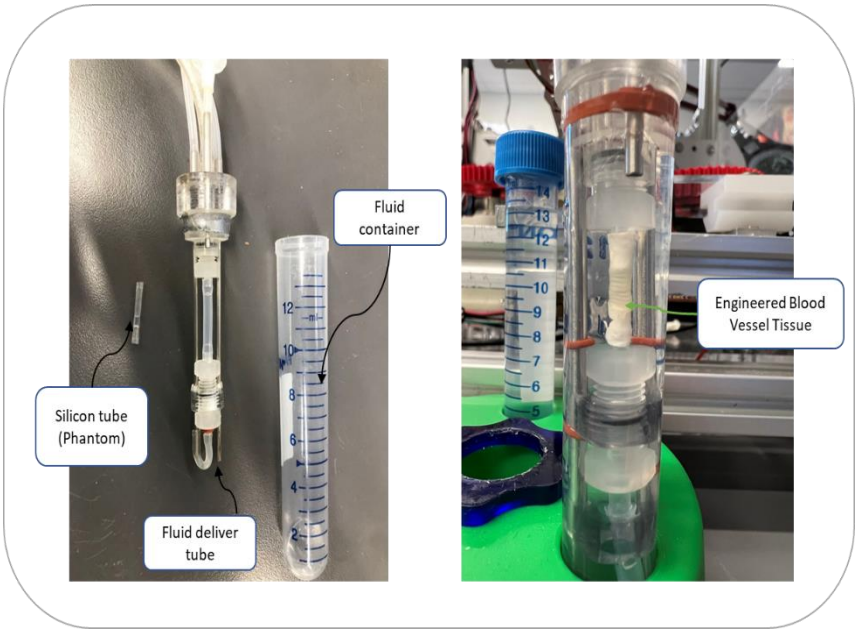

Figure 4. The construction of a luminal flow bioreactor with a pressure loop.

Current evaluation tools like histology and scanning electron microscopy allow us to measure the geometry of the tissue but are destructive [3]. In other words, once these evaluation tools are used to measure the geometry (morphology) of the TEBV, the tissue is destroyed. As a result, the tissue geometry cannot be monitored over time. Therefore, a new, non-destructive evaluation tool is needed to perform serial geometry measurements of the TEBV to monitor tissue development and remodeling. Thus, an imaging monitoring system was proposed to perform serial measurements and observe the TEBV geometry/morphology over time without destroying the TEBV.

1.3 Imaging methods for TEBV

There are several imaging techniques currently used in Tissue engineering. The primary goal is to develop non-destructive methods to evaluate the in vitro production and in vivo integration of engineered tissue implants.[1] Each available imaging technique used to monitor Tissue engineering has its advantages and disadvantages. Each imaging technology is mainly applied in one or more of the three levels of growing complexity.

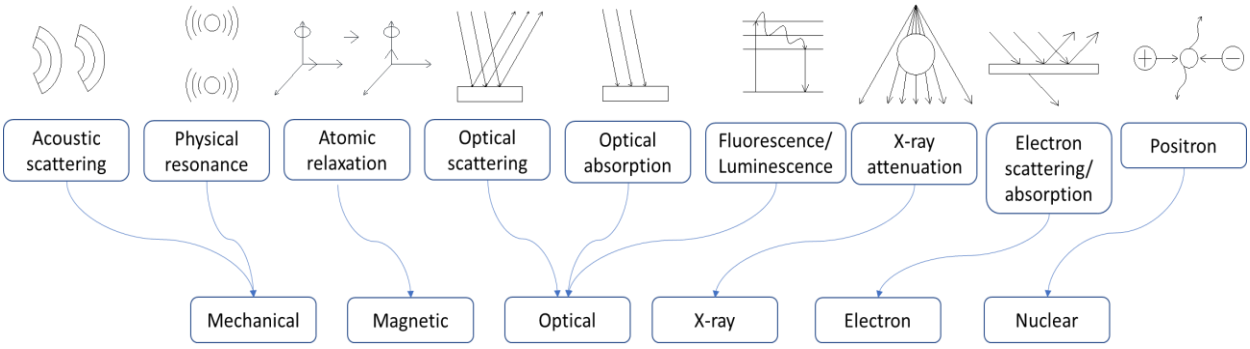

Figure 5. The imaging modalities and the contrast mechanism used in tissue engineering [9].

a. Optical based methods

Current optical microscopy techniques offer a powerful multiscale and multimodal platform to visualize cellular structures down to the nanoscale range. The capability of today's fluorescence microscopy can achieve a nanoscale sensitivity with a resolution (200–400 nanometers). Super-resolved fluorescence microscopy methods allow the capture of images with a higher resolution than the diffraction limit. By coupling with light-sheet, fluorescence microscopy has been extended to thick objects more than 50 µm. This is particularly relevant since the most fundamental building blocks of the cell (cytoskeleton, intracellular membranes, ribosomes, nucleosomes) have sizes and architectural organizations at the nanoscale level, influencing higher-scale cell behavior and differentiation towards tissue and organ development. [1] Optical microscopy includes a wide range of technologies that can be classified in terms of the mechanism of contrast. Optical methods are the most ancient and robust tools for cell and tissue analysis, and their TE applications have been well described during times. The two main categories are fluorescence and label-free (autofluorescence, phase contrast, and second harmonic generation microscopy).[2] They range from classical lens-based microscopy with a light source emitting in the visible spectrum, to fluorescence microscopy, to nonlinear light-matter interactions, such as multiphoton, phase, and second harmonic generation microscopy. Furthermore, nonlinear microscopy also supported several investigation techniques, such as three-photon excitation fluorescence, third-harmonic generation, fluorescence correlation spectroscopy, and image correlation spectroscopy. Today penetration limits and invasiveness problems have been overcome, mainly spreading applicability from in vitro studies, ex vivo verification, including histology, to in vivo skin models for TE (confocal, optical). In some cases, clearing solutions are also used from Optical Computed Tomography. However, computational and adaptive optics approaches can be implemented to minimize sample treatment and the need for 3D imaging.

b. Acoustic based microscopy

Acoustic-based microscopy includes the most promising alternative imaging technologies that take advantage of both ultrasound and optical imaging using optical to ultrasonic energy conversion. It is suitable for showing vascularization and scaffold degradation. The imaging systems, penetration depth, and spatial

resolution are controllable depending on the acoustic and optical design, which increases the application range of photoacoustic imaging from subcellular to whole system level. Furthermore, various options for endogenous and exogenous contrast agents, such as hemoglobin, melanin, metallic nanoparticles, and dyes, are available.[1] PA microscopy has a subcellular level of spatial resolution within a relatively low penetration depth, smaller than 1 mm. PA microscopy is a valuable tool for in vitro 3D non-destructive assessment of Tissue engineering. Ultrasound microscopy, for example, effectively visualizes basic tissue morphology. Although, it is minimal for quantitative measurement of the properties of tissue mechanics because the contrast of soft tissue is limited to a small range of the mass. Nevertheless, these technologies have high biocompatibility, excellent temporal resolution, reasonable penetration depth, portability, and low cost, allowing various applications from small-sized scaffolds to clinical research.[2]

c. Magnetic resonance-based methods

Magnetic resonance technology allows excellent contrast between various soft tissues and has been used to obtain anatomical, functional, and cellular information. Magnetic resonance imaging (MRI) has significant advantages, including no need for ionizing radiation, unlimited penetration depth, high spatial resolution, and excellent clinical utility. They are not the best tools to monitor molecular interactions compared to other molecular imaging modalities. However, because of low sensitivity and limited molecular probes, it is unusual that MRI can visualize and evaluate tissue engineering constructs without exogenous contrast agents, thus in a non-perturbing way, both in vitro and in vivo. MRI includes an extensive arsenal of methods to characterize tissues functionally, particularly for the non-invasive characterization of vessels. MRI could provide a complimentary and real-time quantitative evaluation of engineered tissue growth at all stages, from cells seeding pre-implantation constructs to preclinical validation and post-implantation studies in large animals and humans. [1] Compared with other molecular imaging modalities, its poor sensitivity can lead to long acquisition times and the requirement of large amounts of imaging agents, except for targets within the vasculature.

d. X-ray based methods

X-ray imaging provides detailed 3D information on tissue structure but has limited potential for soft tissue samples.[1] X-ray techniques based on phase contrast are up-and-coming to overcome this limitation in Tissue engineering because of their excellent spatial resolution and high tissue penetration depth. Conventional X-ray techniques are exceptional for imaging soft tissues and biomaterials without the need for contrast agents. X-ray-based methods are also helpful for surface properties parameterization, essential for the success or failure of a biomaterial device. Furthermore, many tools are available today to perform X-ray analysis under controlled temperature and humidity conditions.

e. nuclear imaging

Positron Emission Tomography (PET) and Single-Proton Emission Computed Tomography (SPECT) allow "end radiology"-based analysis. They measure radiology emitted by an endogenous source instead of an external X-ray emitting source. [1] These technologies are helpful in the clinical field, are often coupled with MRI and CT, and are mainly used for tumor progression monitoring. PET and SPECT are the most sensitive molecular imaging techniques. They help track stem and progenitor cells delivered in vivo to monitor cell function and localization within the body. However, SPECT is less quantitative and sensitive than PET. By using radioactive agents, which can be localized in specific organs or tissues, specific chemicals of biological interest can be radio-labeled, allowing nuclear imaging to monitor functional processes. These imaging modalities are mainly used in multimodal imaging approaches rather than direct imaging.

f. Ultrasound based methods

Several imaging modalities are available to examine the morphological, functional, and molecular features of engineered tissues in small animal models. Ultrasound imaging has significant attention due to its ability to exploit the strong contrast and the high spatial resolution without emitting radiation. Applications of the US relevant to tissue engineering include stem cell tracking, monitoring scaffolds in vivo, and evaluation of vascularization. In addition, the emerging capabilities of Ultrasound technologies applied to the detection and monitoring of cancer and other inflammatory diseases could be exploited by tissue engineers [6]. Ultrasound imaging is based on the generation and reception of sound waves as they penetrate materials and are partially reflected at interfaces between tissues of different densities of acoustic impedance. Ultrasound imaging uses a probe to transmit and receive sound waves that must be placed in front of the tissue and requires a computer to process the image. Tissues with different impedance result in gray-scale contrast in the reconstructed image. The typical spatial resolution of ultrasound can be as small as 0.1 mm, and with higher ultrasound frequency, spatial resolution increases, although the depth of penetration is limited. Ultrasound has a great temporal resolution, capable of displaying images in near-real-time 24 Hz to 120 Hz but has difficulty penetrating hard materials such as bone. Although ultrasound imaging is most often utilized to assess constructs near the skin non-invasively, alternate probe designs allow for more invasive assessments such as intravenous ultrasound, transesophageal echocardiography, and transvaginal ultrasound. However, as the acoustic impedance of tissue is similar across tissue types, ultrasound generally has poor contrast, and it is challenging to differentiate nearby structures, especially when compared to X-ray and MRI. Image 2 shows the ultrasound image in different configurations.[19]

g. Ultrasound Computer tomography-based methods

Computed tomography is where the transducer is rotated around the testing material. The properties of the ultrasonic transducer frequency level, the value of the angle beam, and the maximum input voltage are selected based on the purpose of application [4]. The frequency level is one of the main properties to be considered. The range of 100 kHz–1 MHz is categorized as a medium frequency level. The selection of frequency levels depends on the applications, emphasizing resolution or penetration level. A high frequency provides high spatial resolution but a limited depth of penetration. Low frequency offers a greater depth of penetration but lower spatial resolution. The low-frequency range is from 2 to 5 MHz in the medical field, and the high-frequency range is 10 to 15 MHz [4].

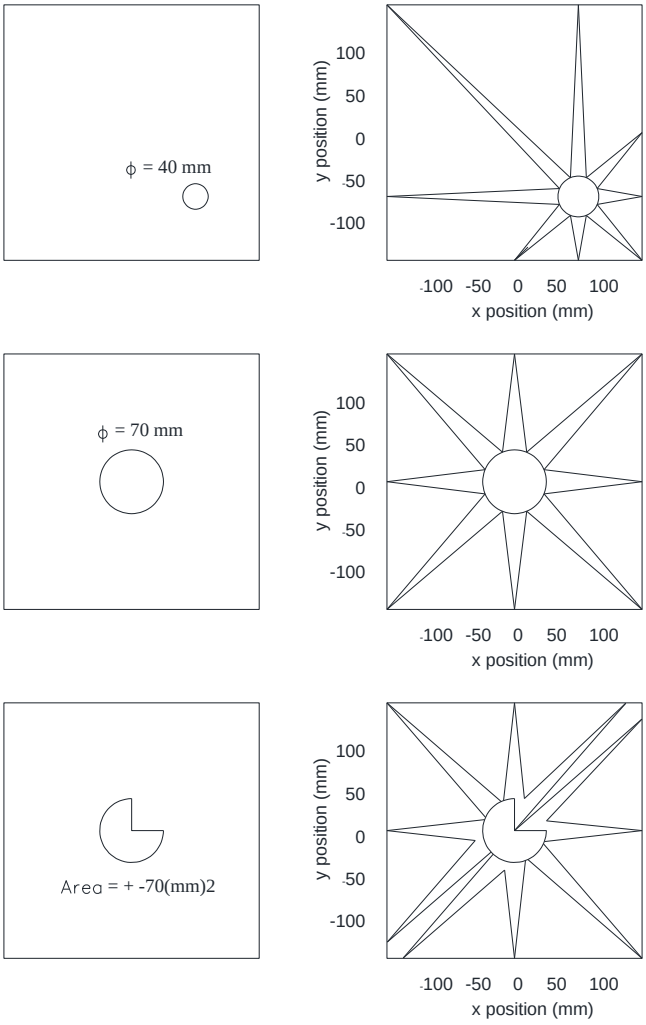

Figure 6**.** In ultrasound computer tomography scanning technology, the image shows a region with different locations, sizes, and shapes [4].

Ultrasound computer tomography technology was published in the early 1980s [2]. Several scientists have been working on ultrasound tomography [2], and there are many studies for using ultrasound computer tomography systems for different applications. One example is 3D imaging of the female breast. There is a successful Ultrasound Computer Tomography device for breast scanning in a clinical application nowadays. However, designing a device to use Computer tomography principles for imaging Tissue engineering was never done before.

1.4 Properties of the biomedical imaging modalities

Biomaterials have played crucial roles in biomedicine by serving as scaffolds to support engineered tissue and carriers to deliver bioactive agents and therapeutic molecules in precision medicine [9]. Therefore, it is important to visualize biomaterial–tissue interactions with minimal invasiveness and fidelity [9]. However, imaging biomaterial–tissue interactions have always been challenging because it usually requires proper imaging contrast to be engineered into the biomaterials and the cells. Moreover, it becomes even more challenging in vivo settings due to the increased need for imaging depth, complex tissue environment, and interference from the functioning biological system. Therefore, modern biomedical imaging modalities are

built to image biomaterials with significantly enhanced spatial resolution, penetration depth, temporal response, detection sensitivity, and chemical specificity. On the other hand, engineering approaches have been advanced to endow biomaterials, and cells with novel contrast mechanisms, enabling the characterization of biomaterial–tissue interactions at relative ease.

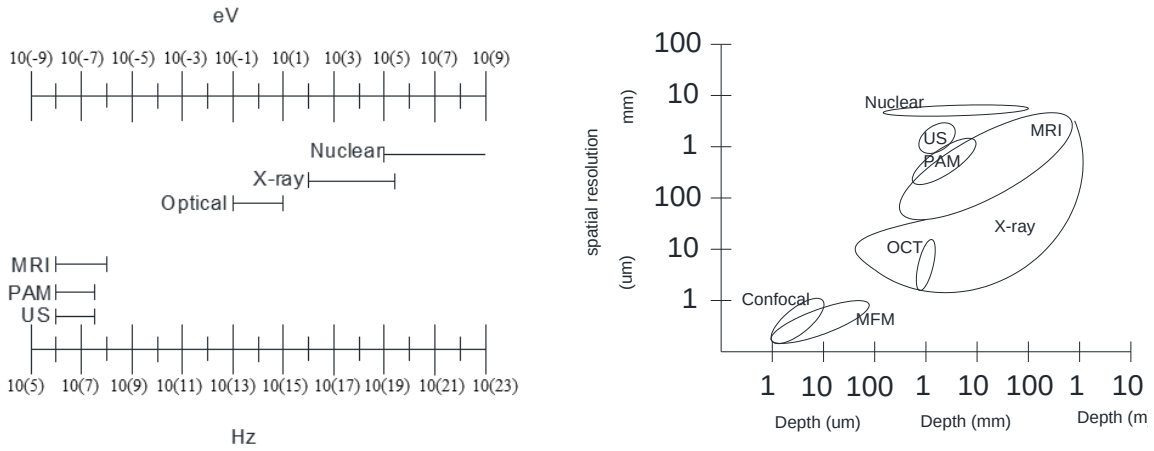

Figure 7**.** The first image shows the range of energies/frequencies on the electromagnetic spectrum used by 3D imaging modalities. The second image shows approximate spatial resolution ranges and imaging depth achievable by imaging modalities [9].

All biomedical imaging modalities rely on the interactions between the applied probing energy format (for example, light, sound, magnetic field, or X-ray photon) and the biomaterials. These interactions generally include absorption, scattering, and polarization of the probing energy by the objects. Therefore, there are many criteria for group imaging technologies, such as resolution, imaging depth, and contrast mechanism. Table 1 shows the property Summary of some of the Biomedical Imaging Modalities used for Tissue engineering monitoring [9].

Table 1. Properties of the biomedical imaging modalities [9].

Imaging modality	Contrast mechanism	Typical spatial resolution	Typical penetration depth	Approximate scan time (Latency)	Type of Image method	Advantages	Disadvantages	Representative applications
USCT	**Acoustic reflection (backscattering)**	**0.3 mm**	**10 cm**	**Almost Real-time**	**Non-destructive**	**Non-invasive, high speed, deep penetration**	**Low resolution, low chemical sensitivity, coupling medium needed**	**Mechanics, flow dynamics, scaffold cavitation**
MRI	Proton magnetization and relaxation	1 mm	50 cm	1 minute – 20 minutes	Non-destructive	Non-invasive, deep penetration	Expensive, low imaging speed	Fluid content and transport
MPM CM	Fluorescent emission, optical scattering	1 μm	1 mm	10E-9 seconds	Non-destructive	The non-invasive, cellular-level resolution, high chemical sensitivity	Superficial penetration	Cell attachment of scaffolds, gene expression
OCT	**Optical backscattering**	**10 μm**	**2 mm**	**minutes**	**Non-destructive**	**The non-invasive, cellular-level resolution, high imaging speed**	**Superficial penetration, low chemical sensitivity**	**Vascularization, cell tracking, scaffold degradation**
PAT	Optical absorption	0.1 mm	10 cm	- (No data)	destructive	Non-invasive, high functional and chemical sensitivity, deep penetration	Coupling medium needed	Vascularization, oxygenation, cell tracking, cell–biomaterial interaction
X-ray imaging	X-ray absorption	0.1 mm	40 cm	Seconds – 10 minutes	destructive	Non-invasive, deep penetration, high resolution	Ionizing radiation, low chemical sensitivity	Engineered bone, pore structures
TEM/SEM	Electron scattering or diffraction	1 nm	0.1 μm	- (No data)	Non-destructive	Nanoscale resolution	Invasive (needing sample fixation), complex sample preparation, superficial penetration	Cell–biomaterial interaction, mineralization
PET/SPECT	Gamma-ray emission	5 nm	50 cm	10^{-12} seconds	destructive	Non-invasive, deep penetration, high molecular sensitivity	Low resolution, radiative labeling	Cell metabolism, cell tracking

Common biomedical imaging modalities can be classified as acoustic, magnetic, optical, electron, X-ray, and nuclear imaging by their contrast mechanisms. We discuss each type of imaging modality for potential use in characterizing biomaterial–tissue interactions, sorted by their probing energies from low to high.[9]

Why USCT?

We need an imaging system that targets the TEBV inside the bioreactor (a closed system retains sterility during serial measurements). However, the cylindrical shape of the bioreactor, different cell sources, chemical stimulation (different fluid), and the need to monitor the tissue at all its length make it difficult to use an imaging system. There are two suitable options for monitoring TEBV inside a bioreactor. OCT – optical coherence tomography and USCT – ultrasound computer tomography. Table 1 shows the properties of OCT and USCT image modalities. Both image modalities can perform a circular imaging motion and, based on table 1, can image TEBV inside the bioreactor. OCT – uses optical backscattering as a contrast mechanism. It has a 10 μm spatial resolution, the penetration depth is 2mm, the scan time is almost minutes, and it is non-destructive (zero-emission radiation). USCT - uses acoustic reflection (backscattering) as a contrast mechanism. It has a 0.3 mm spatial resolution, the penetration depth is 10 cm, scan time is almost real-time, and non-destructive (zero-emission radiation). One study uses an optical coherence tomography (OCT) non-destructive images system as an evaluation tool to obtain the geometry of TEBVs. The paper demonstrates a non-destructive and real-time imaging strategy to monitor the growth and remodeling of TEBVs by using optical coherence tomography (OCT) [12]. However, an imaging system in clinical application is not readily available for monitoring TEBV. Therefore, we proposed an ultrasound computer tomography imaging system that provides an alternative way to the need for non-invasive TEBV growth monitoring. Both systems have pros and cons, but compared to optics-based imaging modality, ultrasound computer tomography imaging is easier to set up the system and requires less computational power and much less for the same application (less than five thousand dollars). The proposed prototype consists of a single-element transducer that moves in a circular trajectory and collects A-lines of the cross-section of the Tissue-engineered Blood Vessel. Additionally, a reconstruction algorithm is used to reconstruct the image from the acquired data.

1.5 Problem statement

As shown in section 1.1, to fabricate TEBV, we need tissue cells, feeding fluid for the tissue, a bioreactor, and an incubator. The bioreactor creates the condition for tissue to grow, and the fluid circuit pumps carbohydrates and oxygen to feed the TEBV inside the bioreactor shown in figure 8. Furthermore, the bioreactor is connected to the fluid circuit and is placed in an incubator at 37°C to stimulate tissue growth. A fully grown tissue from a luminal flow bioreactor typically needs several weeks to fabricate. Current evaluation tools like histology and scanning electron microscopy allow us to measure the geometry of the tissue but are destructive [3]. In other words, once these evaluation tools are used to measure the geometry/morphology of the TEBV, the tissue is destroyed. As a result, the Tissue geometry cannot be monitored over time. Therefore, a new, non-destructive evaluation tool is needed to perform serial geometry measurements of the TEBV to monitor tissue development and remodeling. Thus, an imaging monitoring system was proposed to perform serial measurements and observe the TEBV geometry/morphology over time without destroying the TEBV.

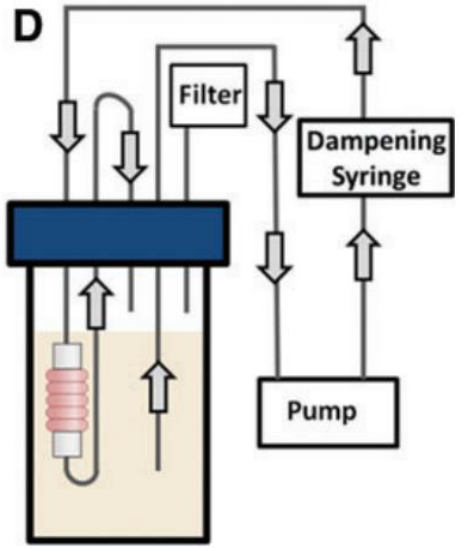

Figure 8. The fluid wiring schematic of the bioreactor during culture. [3] Reproduced with permission [3].

We proposed an Ultrasound Computer Tomography (USCT) Imaging system that provides an alternative way to achieve non-invasive TEBV growth monitoring. The design of the USCT imaging system was based on the TEBV fabrication circuit. When performed imaging, the bioreactor cannot be rotated (it needs to be fixed), and it can have different fluids inside (MDEM, PBS, and sometimes water). In addition, the size and length vary on the model type of the fabricated TEBV. The live TEBV can stay out of the incubator for around 35 minutes when connected with the fluid pump and around 10 minutes when the fluid pump is not connected. To facilitate the work in this study, we used only the fixed cell TEBV inside the bioreactor.

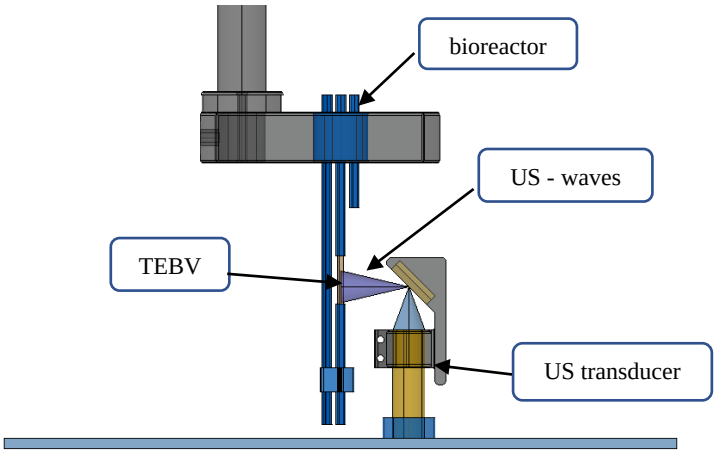

Figure 9. US transducer scanning the TEBV.

Based on the TEBV and bioreactor conditions, the system was designed to have a single element transducer that moves in a circular trajectory along the bioreactor to perform imaging and collect A-lines of the cross-section TEBV shown in figure 9. A back-projection algorithm is used for imaging reconstruction from acquired A-lines. This USCT device aims to perform imaging on a TEBV, show the cross-section of the TEBV, get the geometric parameter of the TEBV (inner diameter (ID) and outer diameter (OD)), and calculate the wall thickness (Wth) shown in figure 10 c). Moreover, to find which fluid is better to use for imaging the TEBV inside the bioreactor.

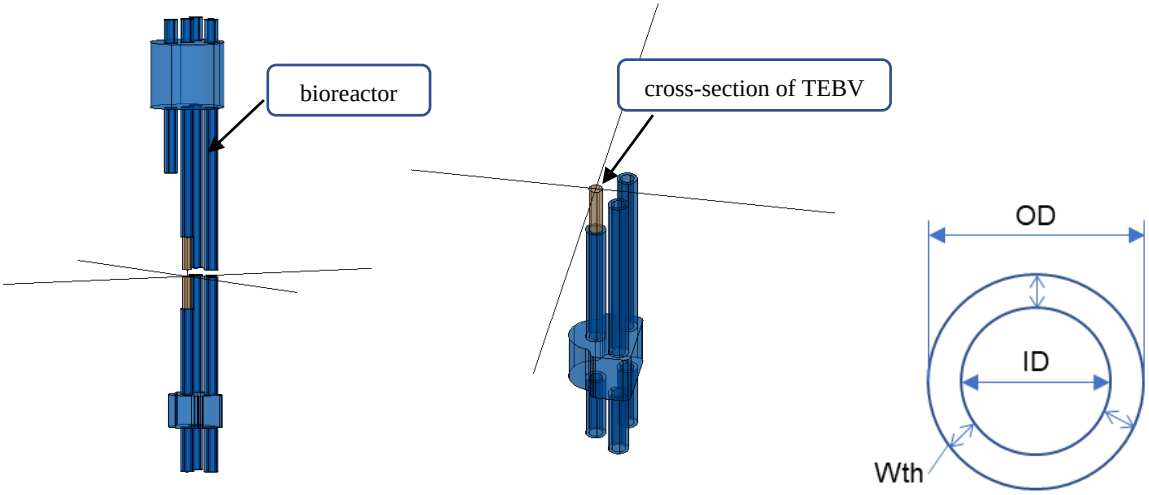

Figure 10. a) 3D model of the bioreactor with TBVE inside (the yellow cylinder represents the TEBV, b) 3D model of the bottom half of the bioreactor (simulate the scanned section), c) the cross-section of the TEBV.

We built the prototype to perform ultrasound tomography imaging of the TEBV inside the bioreactor. We developed the data acquisition to perform imaging and acquired A-lines and reconstruction algorithm to reconstruct the image from the acquired A-lines shown in figure 11. Experiments were conducted to validate the imaging system, and a needle phantom was used to evaluate the point spread function (PSF)

and the device's measurement accuracy. After the device was validated, the experiments continued with the imaging of the TEBV inside the bioreactor. From the acquired images, we could see and perform geometric measurements of the cross-section of the tissue-engineered blood vessel. To verify the geometric measurements done from the device, the TEBV was processed for histology and measured TEBV wall thickness. The result of the TEBV wall thickness from the plot and the histology were compared to evaluate the measurement error of the USCT device.

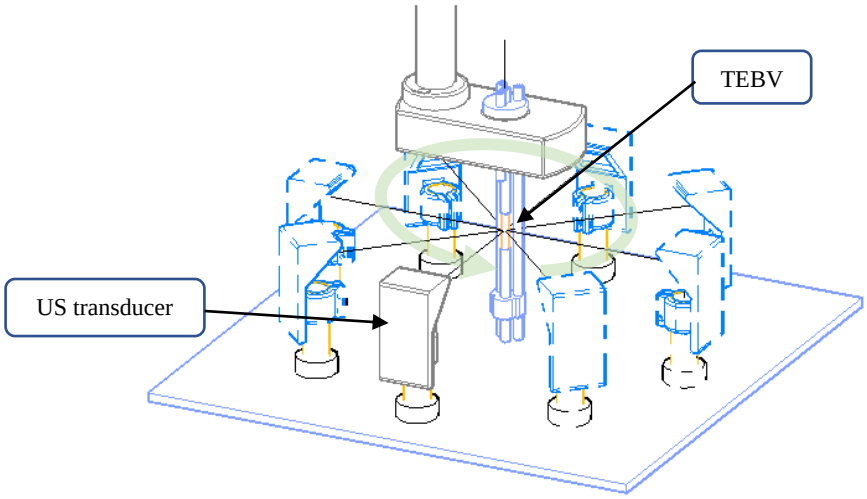

Figure 11. The 3D concept of USCT imaging TEBV.

The last validation of our system is the TEBV fluids validation. The goal was to find which fluid is better to use on the bioreactor when performing imaging. We perform imaging of the TEBVs in all three different fluids (PBS, DMEM, water) and calculate each fluid's signal-noise ratio (SNR). The fluid with the high number is the best fluid to use for image TEBV.

2. Hardware and Control

2.1 The mechanical *overview of the designed prototype*

The USCT-designed prototype consists of five major parts (shown in figure 12): the frame, the water container, ultrasound transducer with acoustic reflector, bioreactor holder and positioner, the rotation transmission shaft, and the control circuit, weight support stainless-steel plate.

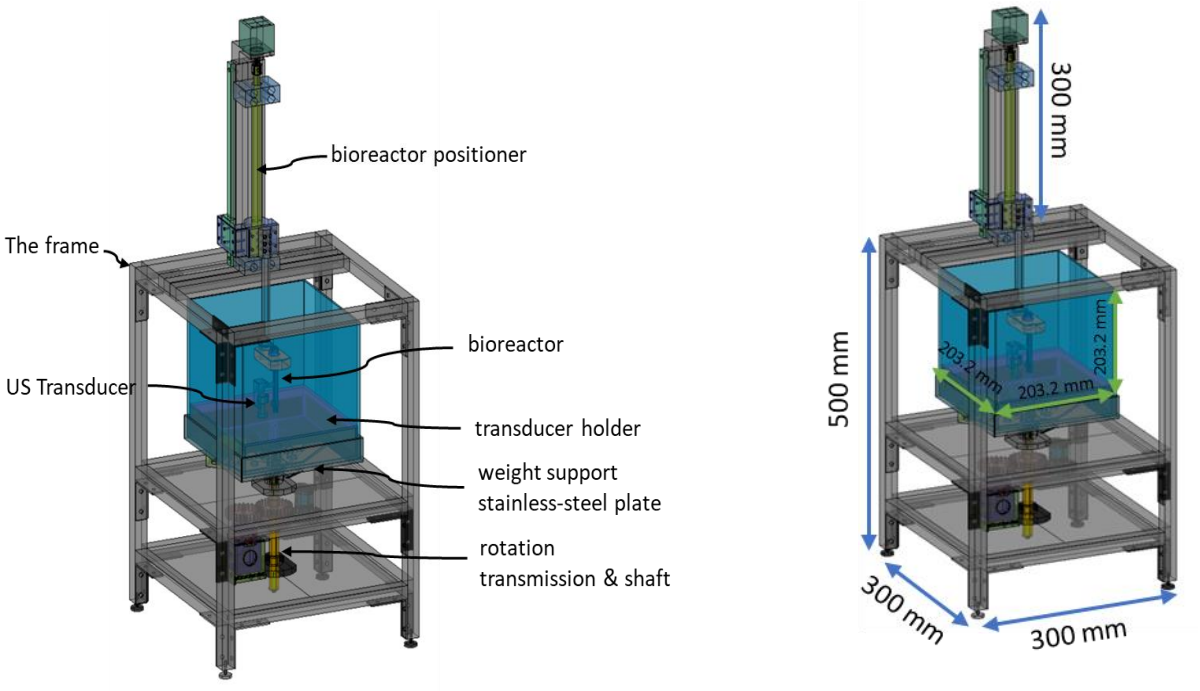

a) b)

Figure 12. a) The 3D design concept of the USCT imaging device, b) the dimension of the frame and the dimensions of the water container.

The device's frame is created from 22 aluminum extruder bars with a dimension of 20x20mm. Four aluminum extruder bars are 500 mm, and the rest are 300 mm. Brackets and corners are used to connect the aluminum extruder and increase the frames' rigidness. The device's measurements are 300 x 300 x 800 mm. The frame is designed to house the water container.

The water container is made from two Cuboid-shaped acrylic boxes with dimensions of 203.2 x 203.2 x 127 mm and 203.2 x 203.2 x 203.2 mm with a thickness of 2.5mm and can hold about 5.3 liters. The large size platform was used to extend the device's capacity to image different types of bioreactors, even animals (rats).

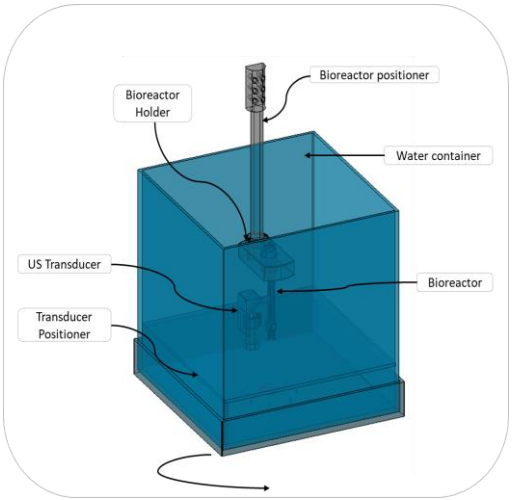

Figure 13. The 3D concept of USCT imaging TEBV.

A 3D printed platform 202.5 x 202.5 x 10 mm installed at the bottom of the container was used to position and hold the transducer. M16 metal cable glands joint is used to make the transducer sensor waterproof. The bioreactor positioner is made of a motor-based 100 mm ball screw stage to move up and down to align and position the bioreactor with the transducer. Note that the ultrasound transducer and the tissue need to be placed into the water to perform an ultrasound scan. A stainless-steel plate with a dimension of 203.2 x 203.2 mm with a thickness of 3.2mm supports the weight of the water container. The device base is installed and fixed on a 30 cm hollow aluminum shaft with a thickness of 3mm and is used as the central rotation axis for the water container. The aluminum rotation hollow shaft has an inside diameter of 10 mm, an outside diameter of 16 mm, and a length of 20 mm. The coaxial cable connecting the transducer and the DAQ (US-Key digitizer) goes through the water container into the hollow to the electrical panel. The rotation is made possible by installing two spur gears on the stepper motor and the aluminum shaft.

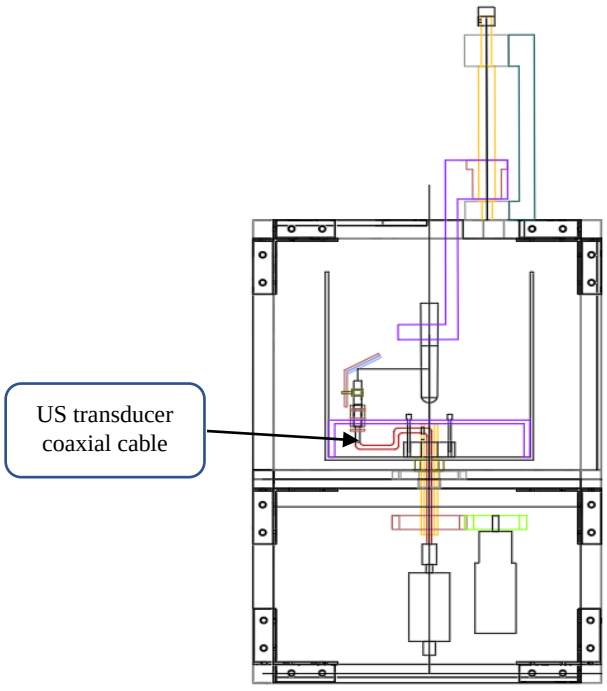

Figure 14. The 2D diagram of how the coaxial cable passes through the water container to the hollow aluminum shaft and connects to the DAQ (digitizer) and the PC.

2.2 Mechanical *Calibration*

We used a level ruler and planar laser leveler to have a steady rotation of the water container to adjust, calibrate, and align the device. Having a stable rotation is very important for the USCT imaging device. Because the ultrasound travels around and gets the cross-section of the TEBV if the rotation is not stable, the measurement of the acquired image will not be accurate, and the image will not be clear. After assembling everything, we started with mechanical leveling, and we used two different leveling rulers shown in figure 15 to level the aluminum frame.

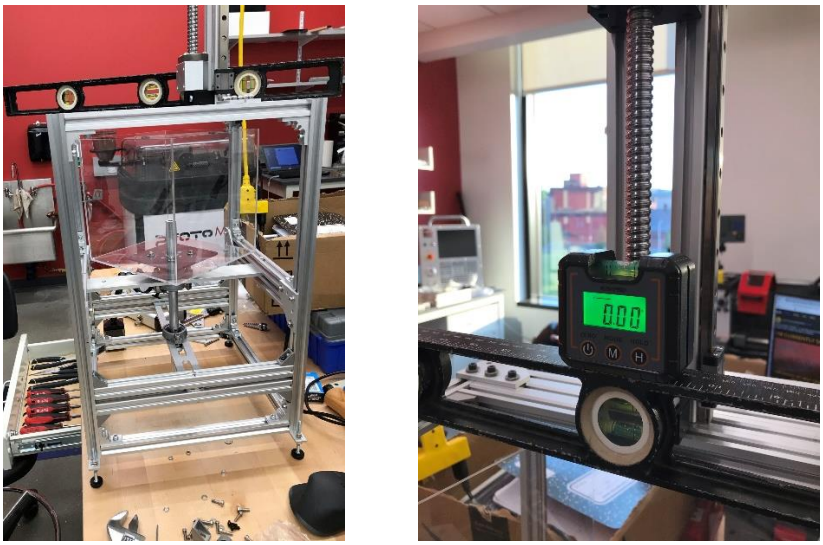

a) b)

Figure 15. The frame leveling

Next, we used the leveling ruler to level the water container and the US transducer position inside the water container.

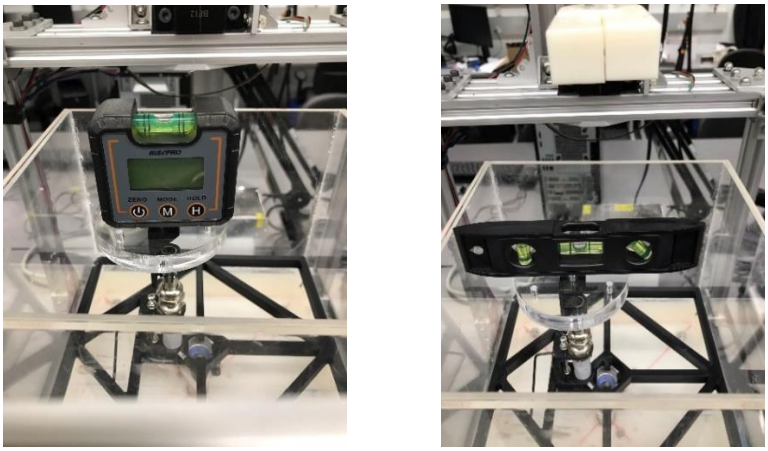

a) b)

Figure 16. The water container and the ultrasound transducer leveling.

As a result, after leveling the aluminum frame and the water container, the deflection of the rotation of the water container is 0.03mm shown in figure 17.

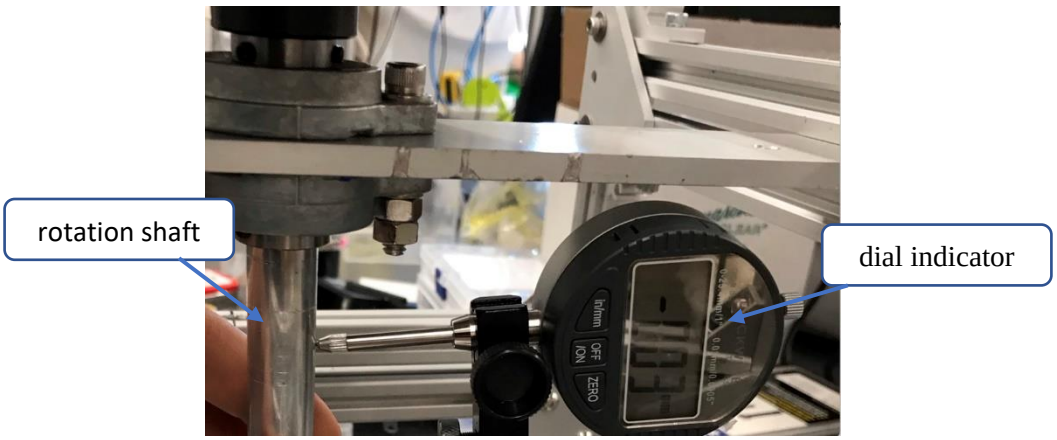

Figure 17. The rotation deflection was measured with the dial indicator instrument.

Another important part of mechanical calibration is the alignment of the transducer positioner concerning the axis of rotation of the water container. We used a laser level with self-leveling and vertical and horizontal lines to align them shown on the image

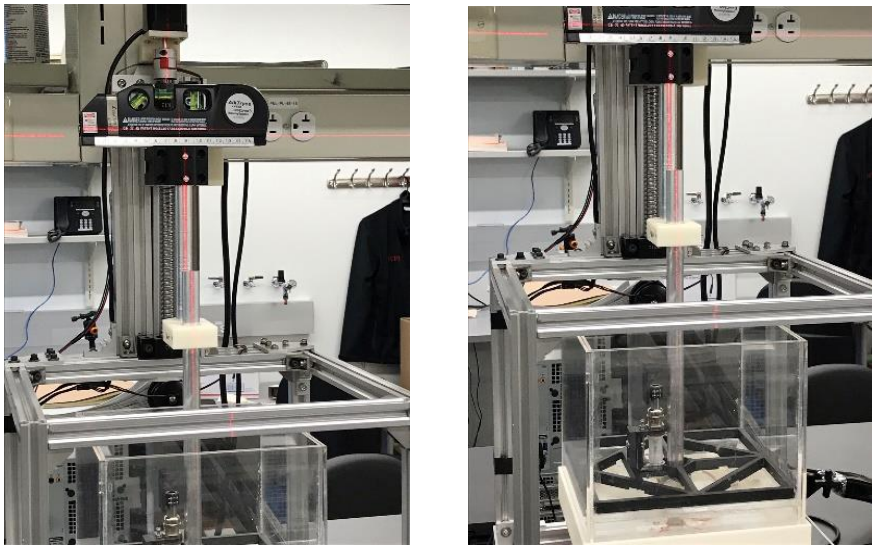

Figure 18. Alignment of the transducer positioner using laser level with self-leveling and vertical and horizontal lines.

2.3 Ultrasound transducer and acoustic reflector/mirror setup

We positioned our sensor vertically and used an acoustic reflector/mirror to redirect acoustic waves. The setup makes it more flexible for different imaging types of bioreactors or even the mice's blood vessels. In addition, acoustic reflectors are commonly used on ultrasound instruments, and they have been proven to have a negligible loss of signal strength. Therefore, we purchased a glass-based acoustic reflector 14x14 mm with a 1.8 mm thickness and mounted it on a 3D printed platform 45-degree angle and 12.6 mm from the transducer shown in figure 19. a). This design will reflect the acoustic wave by 90 degrees into the horizontal plane shown in figure 19. a).

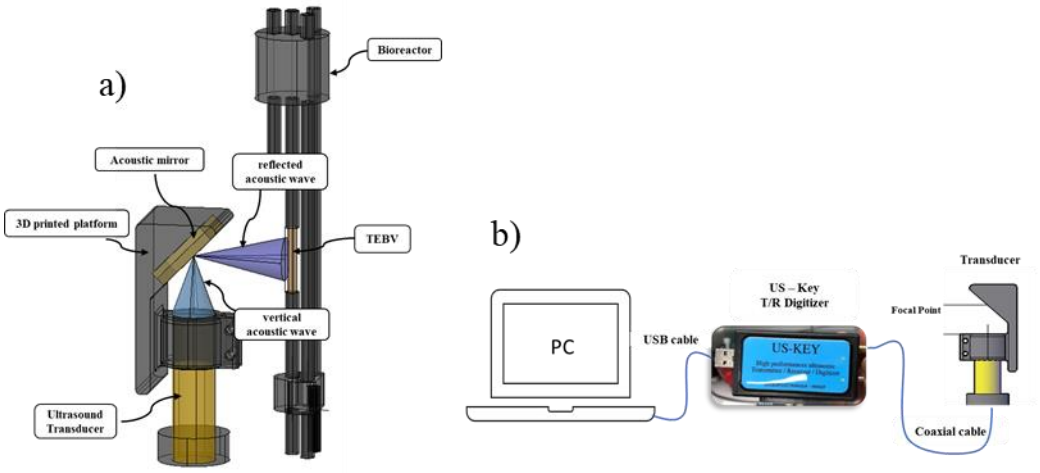

Figure 19. a) The 3D model of the acoustic reflector setup and b) the US PC connection diagram.

The single element transducer generates and receives ultrasound waves. The ultrasound transducer we used has a central frequency of 6MHz and a focal depth of 12.7mm. We used a portable signal generator and acquisition device from Lecoeur Electronique to convert the analog to digital signal from the transducer to the PC and vice versa (figure 19. b)). The sampling frequency of the digitizer is defined to be 80MHz.

2.4 The electric circuit diagram

The device consists of two stepper motors, two stepper motor drivers, one CNC GRBL shield (V.1.1), one encoder, three limit switches, one toggle switch, and one microcontroller.

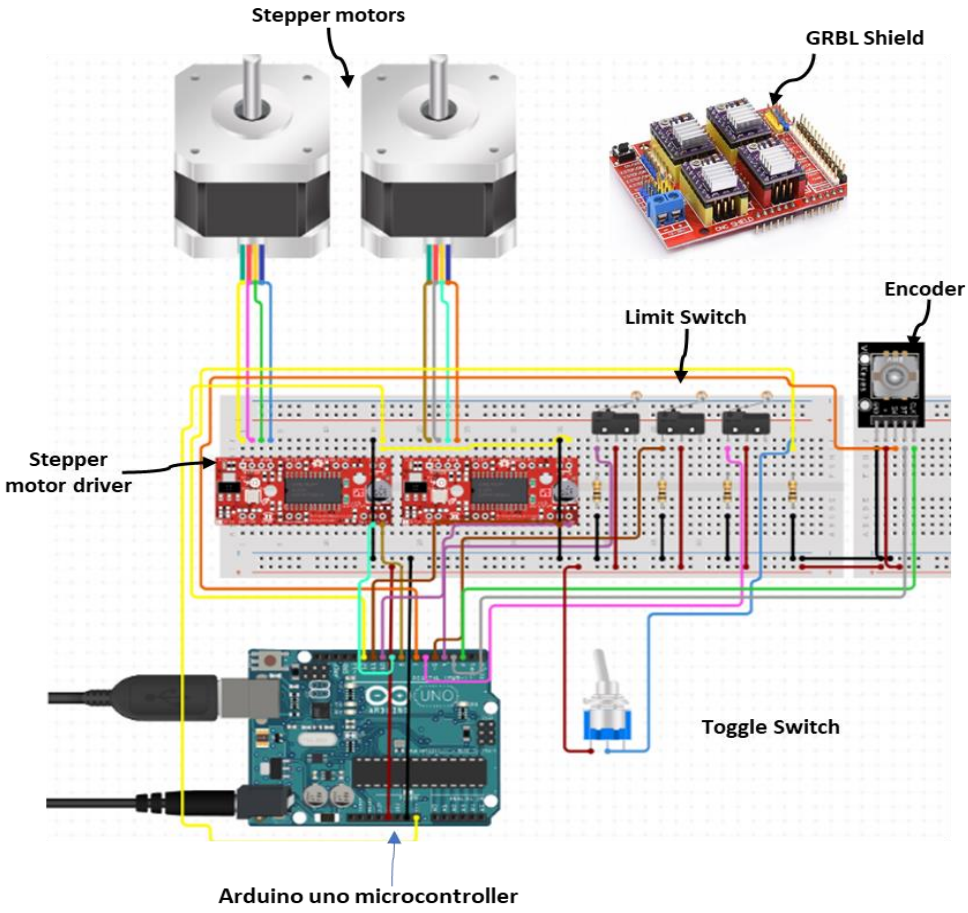

Figure 20. The electrical circuit diagram of the device.

The bipolar stepper motor c1) with planet gearbox (gear ration is 5.18:1) with an 8 mm diameter shaft that has a 1.8 step angle (200 steps/ revolution). It can allow a holding torque of 18 kg-cm (176N-cm), more than enough to move a 5.3-liter water container. The hybrid stepper motor c2) has a 1.8 step angle (200 steps/ revolution) and can hold up to 3.5 kg-cm high torque output. The hall angle sensor e) is a miniature 360 sensor that works on the hall effect principles. The analog output of this sensor is 0 to 5V so that it can be connected directly to Arduino. This sensor works by converting its angle data to an electrical signal. Rotation resolution is: 0.088 degrees (12-bit ADC) with an accuracy of +- 0.3%, and a refresh rate is 0.6ms / 0.2ms in high speed). The open-source microcontroller Arduino Uno board a) is based on the microchip ATmega328P microcontroller developed by Arduino. The Pololu A4988 is the driver b) for stepper motors. It has micro-stepping for bipolar stepper motor driver features and five different micro-step resolutions (1/16-step).

Arduino Uno GRBL Shield is a computer numerical control stepper driver platform that connects the drivers with the microcontrollers. The shield makes it possible to configure the microcontroller compatible with GRBL v1.1 4-axis firmware.

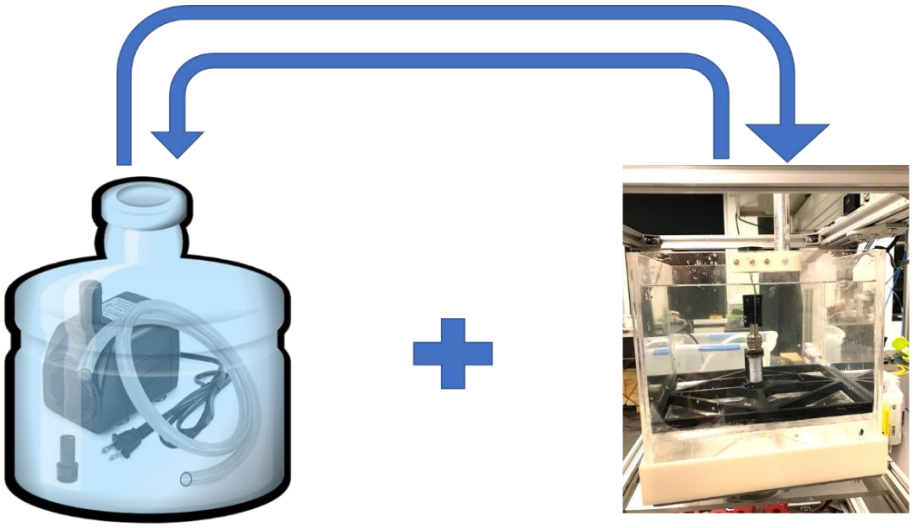

Figure 21. Water pumping in and out of the device container schematic.

The USCT imaging device needs a large amount of water (about 5.3 liters) to perform scanning. Therefore, we purchased a 24-wats water pump to fill and remove the water from the water container. It takes about 2 minutes to fill the water container, and it takes 3 to 5 minutes to remove the water from the water container (the water stuck to the 3D printed platform at the bottom of the water container).

2.5 The data acquisition block diagram

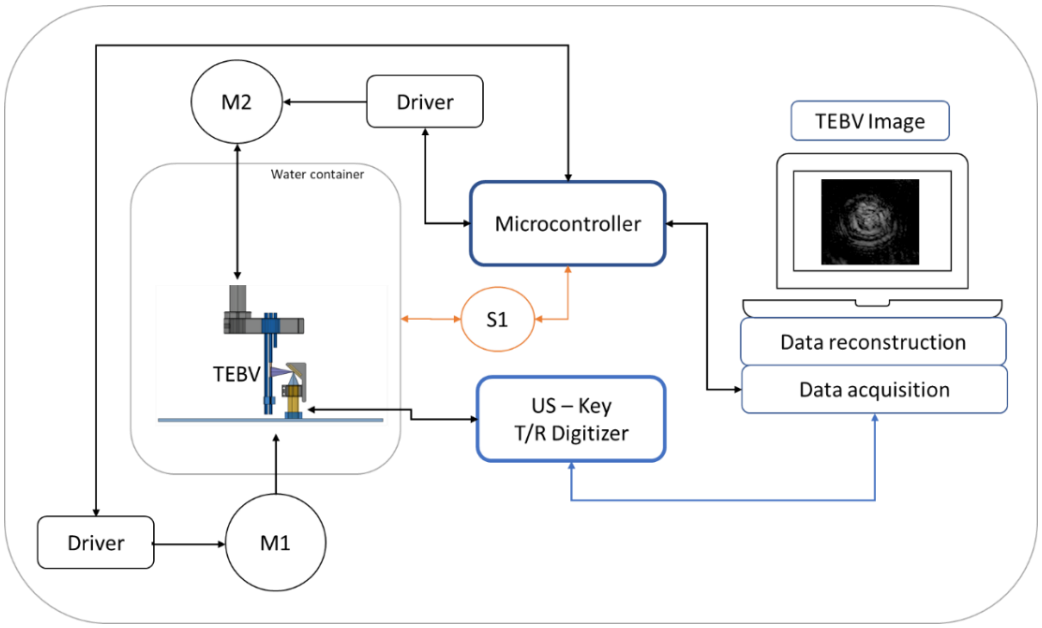

Figure 22. The pipeline of how the device works to acquire the data.

To initiate imaging from the device, the user must follow specific steps. First, MATLAB software must be installed on the personal computer. Second, install the Arduino microcontroller drivers on MATLAB. Third, the US – key digitizer (DAQ) (shown in figure 19. b)) must install on the personal computer and the MATLAB. Fourth, GRBL freeware must be uploaded on the Arduino Microcontroller.

The control algorithm identifies the two serial ports used to communicate with the Arduino microcontroller and US-key digitizer (DAQ). Arduino microcontroller and US-key digitizer have their specific communication port and speed. The algorithm starts by sending a signal to the digitizer to scan the tissue and waits to receive the data shown in figure 23. The data are stored on a temporary memory on MATLAB software.

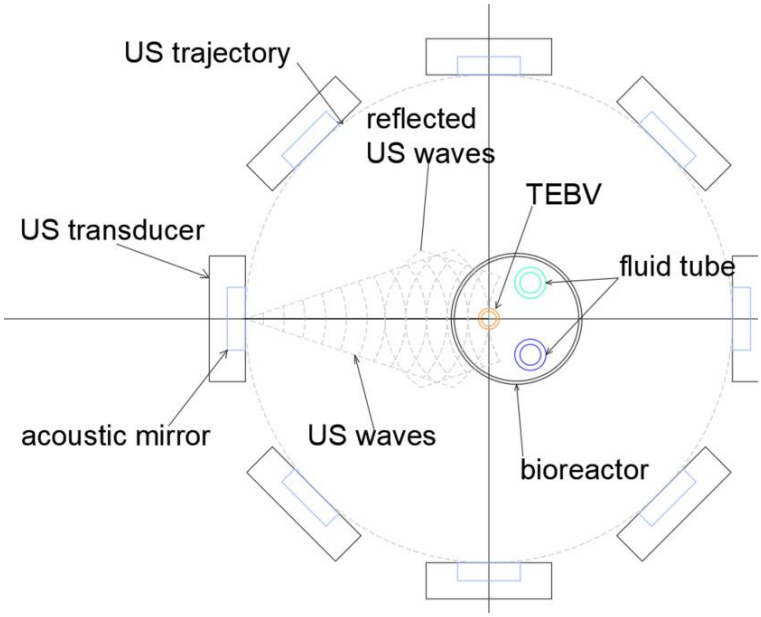

Figure 23. The 2D concept of the US waves generation and reflection.

After getting the data, the algorithm sends a command to the microcontroller to move the motor M1 (shown in figure 22) that rotates the water container 0.5-degree anti-clockwise. This process repeats until the system completes one full revolution 360 degrees, shown in figure 24. When the imaging finishes, the data are stored on a 2D matrix and are ready to be processed. The M2 motor moves and positions the bioreactor based on the target sample. The user can select the different positions and the number of scans (cross-sections) they need to perform. The sensor S1 shown in the image above is used to create a closed-loop control of the motor M1 to increase the imaging resolution. One complete scanning for one cross-section last 28 minutes. After the scanning is complete, the data are ready to be processed.

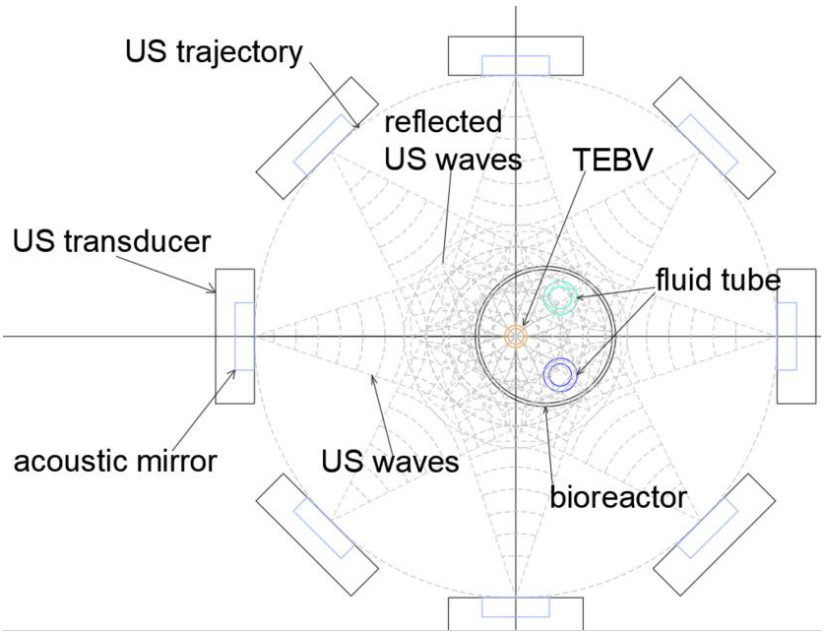

Figure 24. 2D concept of the US waves generation and reflection in a different position.

2.6 The USCT imaging system

The device's water container is filled with water, and the bioreactor is positioned and fixed on the bioreactor holder. The DAQ algorithm is open on MATLAB, and both the Arduino microcontroller and the US-Key are connected to the PC. The device is placed in the home position and is ready to perform imaging shown in Figure 25. When the DAQ algorithm starts and the scanning begins, the A-lines table pops up on the screen. We can see and check from the beginning of the device is scanning or not by checking the A-lines table. If the US wave faces an obstacle and is reflected by the transducer, the A-lines table will change the amplitude signal.

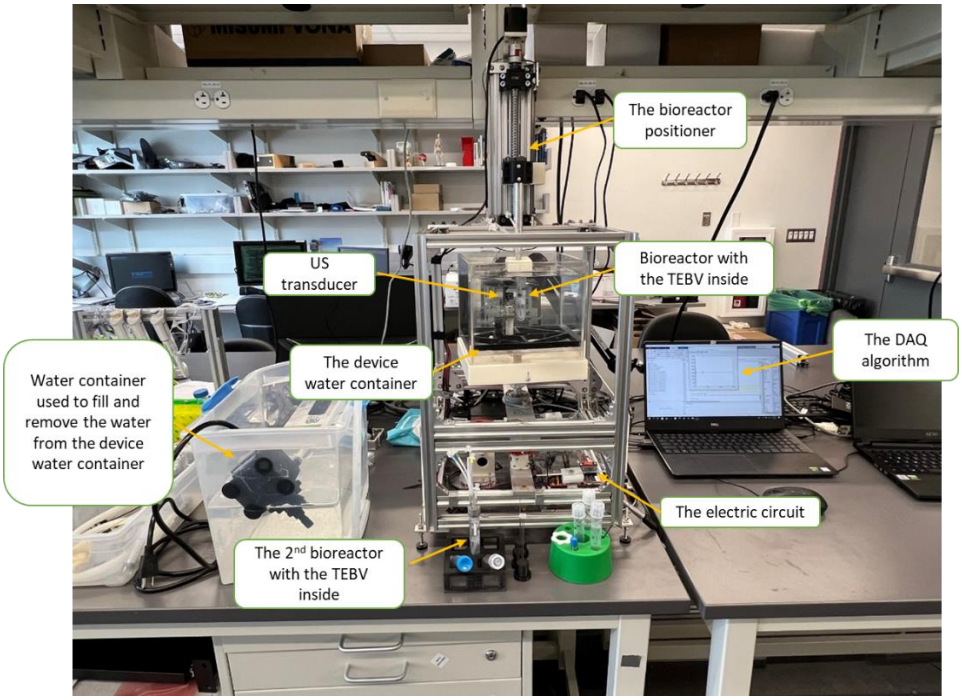

Figure 25. The complete USCT system imaging TEBV inside the bioreactor.

Some environmental factors and conditions can attenuate the US signal and impact the image quality.

- The USCT imaging is affected by the room's temperature because the speed of sound on the water changes when the temperature increases and decreases.
- Noise is the most common factor for the US signal's attenuation, like radio frequencies, electrical currents, and wire leakage. In addition, surroundings like barriers and improper wire installation may distort the transmission.
- The water on the water container should be without bubbles. It is recommended to fill another water container and let it rest for 24 hours to remove the bobbles and then use it for scanning. Note that the water should not be contaminated or stored in the container for long. It will affect the image quality. Before scanning, it is necessary to check it the acoustic mirror is clean.
- It is necessary to need to check the fluid that is inside the bioreactor. This is because different fluids have different sound speeds, so we need to check if the fluid inside the bioreactors has been tested before or check the fluid speed of sound.
- Travel distance is another factor that can affect the US signal's attenuation.

3. Image reconstruction

3.1 Data reconstruction algorithm

The back-projection algorithm is the simplest method for image reconstruction in imaging techniques that require reconstruction from multiple projections. The algorithm calculates the contribution of each voxel (3D pixels data) of the structure to the measured ray data to form an image [5]. Hence the back-projection algorithm forms the B-mode image from the acquired A-lines (acquired 2D – 3D data) shown in figure 26.

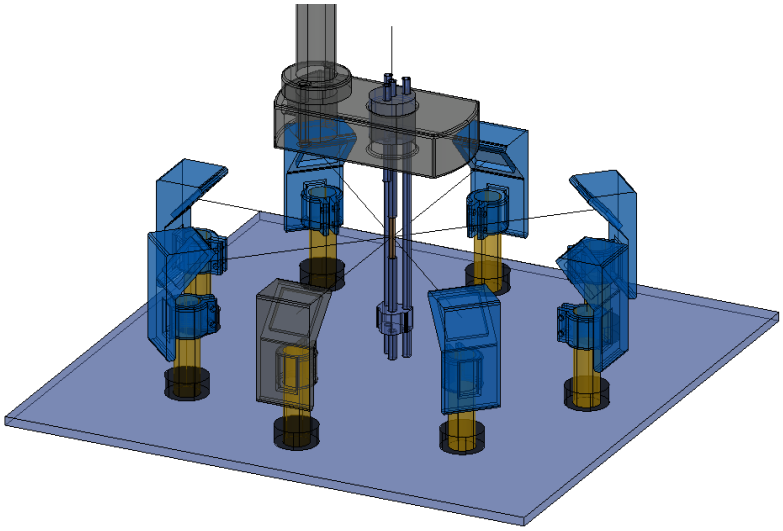

Figure 26. The 3D geometry for image formation.

The algorithm starts by loading the data from the data acquisition algorithm (DAQ). It continues with removing any unwanted signals, for example, high initial signals. If there is any bad data left, we can manually find them and remove them. Then we make sure that the signal zero centers into the x-axis [6]. After finishing with initialization, the algorithm continues with initial parameters like the speed of sound (c), the number of transducers used in this system, (fs)sampling frequency, (r) the distance from the axis of the transducer to the axis of the target sample, focal point (12.7 [mm]). Next, we define the transducer position and the number of step-interval. Step size is computed by dividing the angular field of view and the number of data points taken in one scan. It depends on the data acquired from the DAQ algorithm. We set the device rotation in a clockwise direction. The algorithm checks the number of A-lines that are generated by beamforming.

For this system, we have sound speed = 1430, number of the US elements = 1,
fs = 80 MHz (sampling frequency), r = 20 mm, d = 2*r, step interval = 1, sample spacing = (1/fs) * speed sound * 1000/2, ns = d/ sample spacing, focus sample = focus / sample pacing, step size = (-360/720) * step interval, the new position of the transducer = the new position of the transducer *1000.

3.2 Delay and sum (DAS) beamforming

The algorithm starts with a single element transducer that scans the target phantom/ tissue along a circular trajectory with a radius r, and an angular spacing of $\Delta\theta$. d_k is the length of a segment line between two points (Euclidean distance), from the pixel of interest to the transducer at position k. Next, the focal depth of the single-element transducer is assigned with f. The A-line collected (Ak) on a specific position will be projected into the image space B_{bf} and pixel at (i, j) (figure 27). Last, the aperture growth was implemented as a fixed ratio between signal depth from the transducer and angular aperture size [7]. The equation below explains the pixel value from the back-projection algorithm:

1) $d_k = |p(i,j) - p(k)|$

2) $\mathrm{n} = \left(\frac{2*\pi}{\Delta\theta}\right)$

3) $B_{bf}(i,j) = \sum_{k=1}^{n} A_k * \left(\frac{2*(d_k + f)}{c}\right)$

$\boldsymbol{r}$ - the radius

$\boldsymbol{d_k}$ - the Euclidean distance from the pixel of interest to the transducer at position k

$\boldsymbol{p(i, j)}$ and $\boldsymbol{p(k)}$ - the positions of the pixel of interest and the transducer, in physical space.

$\boldsymbol{\Delta\theta}$ - the angular spacing between neighboring data acquisition positions

$\boldsymbol{f}$ - the focal depth of the single-element transducer

$\boldsymbol{A_k}$ - the collected A-line

$\boldsymbol{B_{bf}}$ - Image space

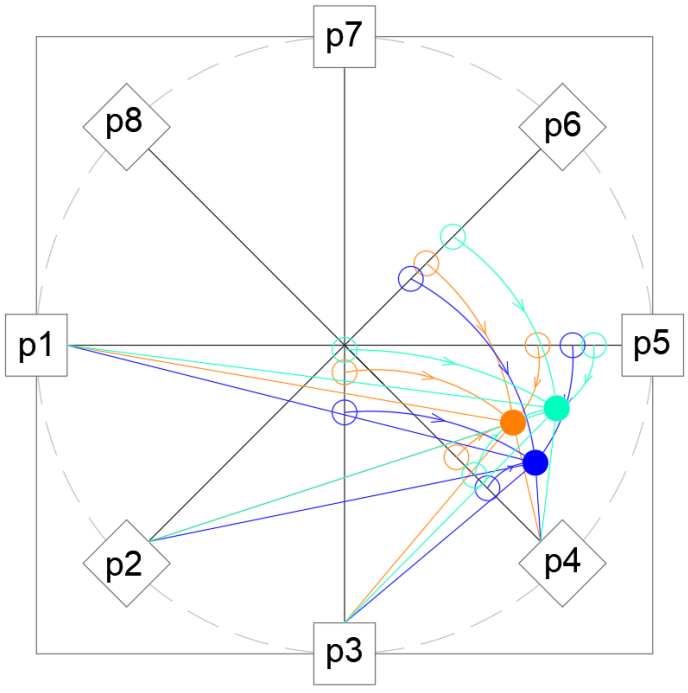

Figure 27. The concept of the back-projected reconstruction method. The solid orange circle represents the TEBV or the pixel of interest, and the hollow orange circle represents the values back-projected of the TEBV. The same is for the solid blue circle and solid cyan circle. They represent bioreactor fluid tubes (pixels of interest), and the hollow circle represents their values back-projected.

After the beamforming is finished, we use envelope detection using Hilbert transform. Hilbert transform is used to create the analytic signal of the input. An analytic signal is a complex signal, where the real part is the original signal, and the imaginary part is the Hilbert transform of the original signal.
After the Hilbert transform, the algorithm use normalization to scale the signals and logarithmic compression to reduce the signal's dynamic range to have better image visualization. Finally, we have reconstructed image the B-mode image shown in figure 28.

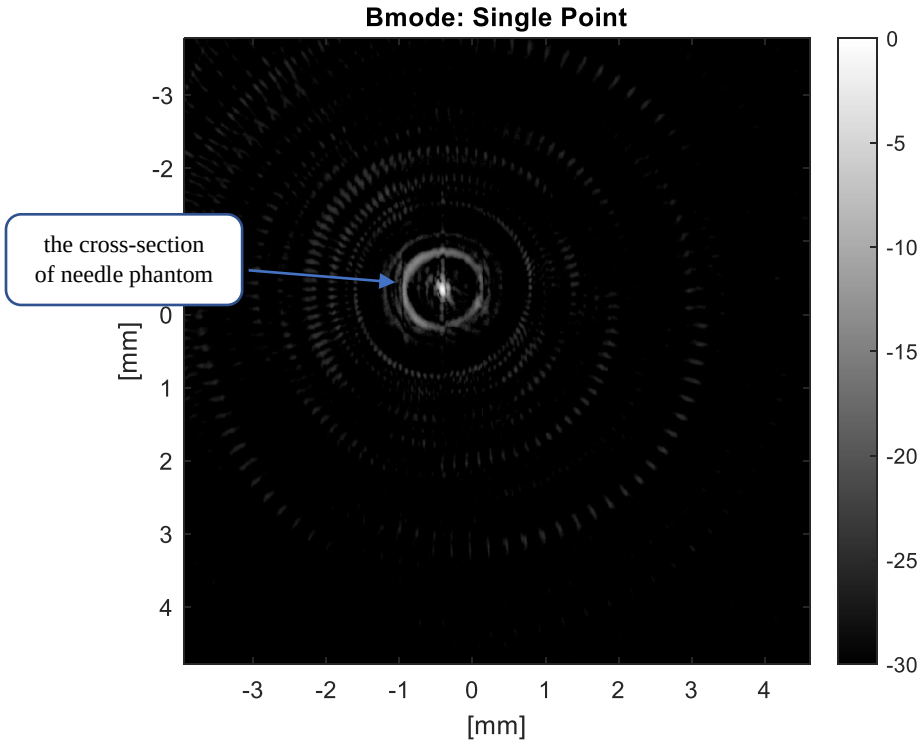

Figure 28. The acquired B – mode image of a phantom needle.

B-Mode is a two-dimensional ultrasound image display composed of bright dots representing the ultrasound echoes. The brightness of each dot is determined by the amplitude of the returned echo signal.

3.3 Partial data back-projection algorithm

Inside the luminal flow with a pressure loop bioreactor is shown in figure 4. It has the TEBV and the two metal fluid tubes. Because the metal has high acoustic impedance, the contras of the reflected signal from the TEBV that we want to image, we used a partial data back-projection algorithm to overcome this issue. The partial data back-projection algorithm is based on the construction of the tissue and is applied to the 2D data matrix we acquired from DAQ algorithms. The 2D matrix axis is the number of samples and the of positions. In this case, we have 15000 samples with 720 positions with a step size of 0.5. The partial data back-projection algorithm uses half of the data from the acquired A-lines to increase the contrast of the phantom/tissue by removing the other half. In other words, the algorithm selects four halves of the bioreactor to see which half presents a better B-mode image—figure 29. Show the direction of the selected partial data of the cross-section of the bioreactor.

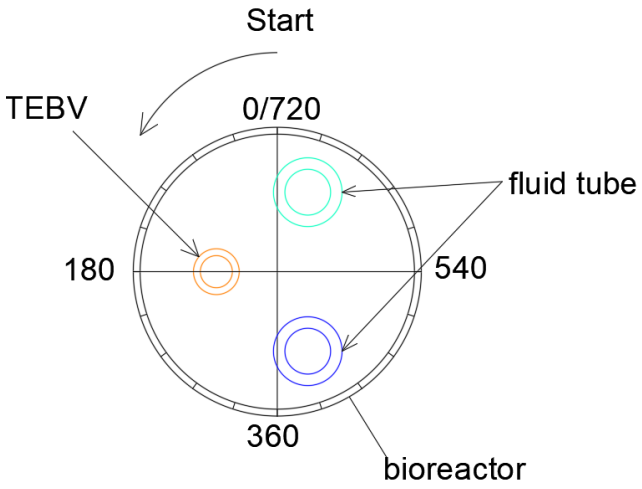

Figure 29. The 2D concept of partial data back-projection algorithms (in degree).

The partial data starts with 0° – 360° first half, then 180° – 540° in the second half, after 360° – 720°, and in the third half and fourth half, we have 540 – 180. Shows in the figures below the highlighted part of the removed data. (The highlighted region is the removed data).

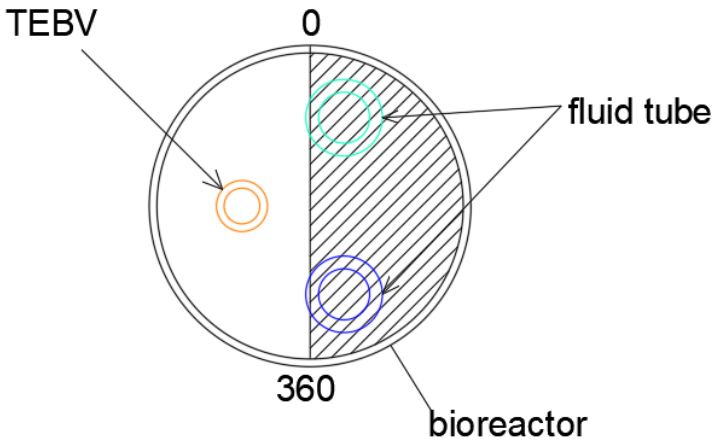

Figure 30. The first half includes 0° – 360°.

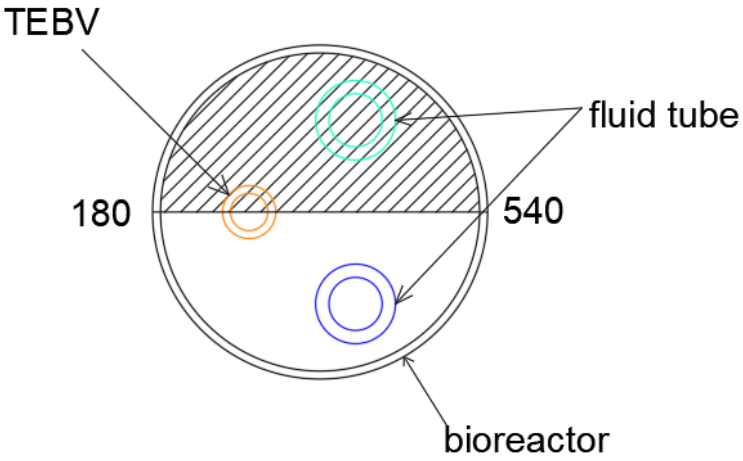

Figure 31. The second half includes 180° – 540°

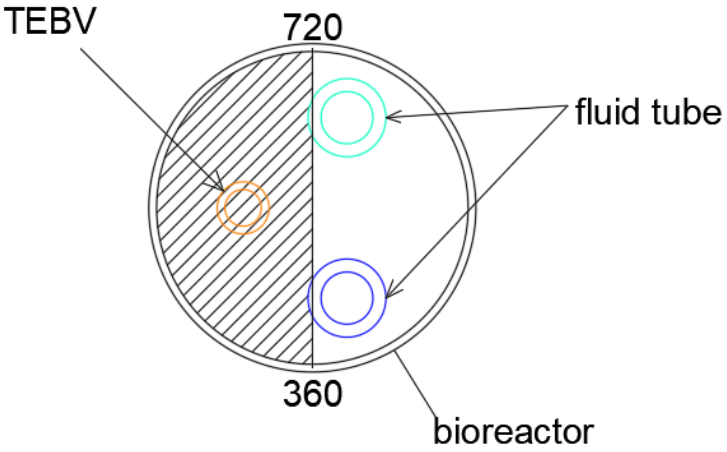

Figure 32. The third half includes 360° – 720°.

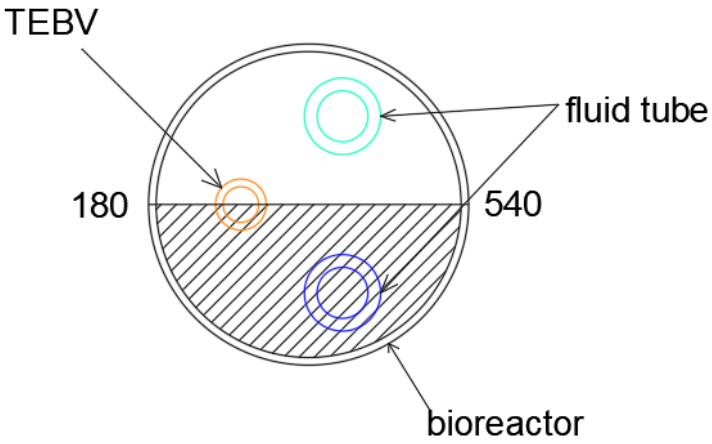

Figure 33. The third half includes 0° –180° and 540° –720°.

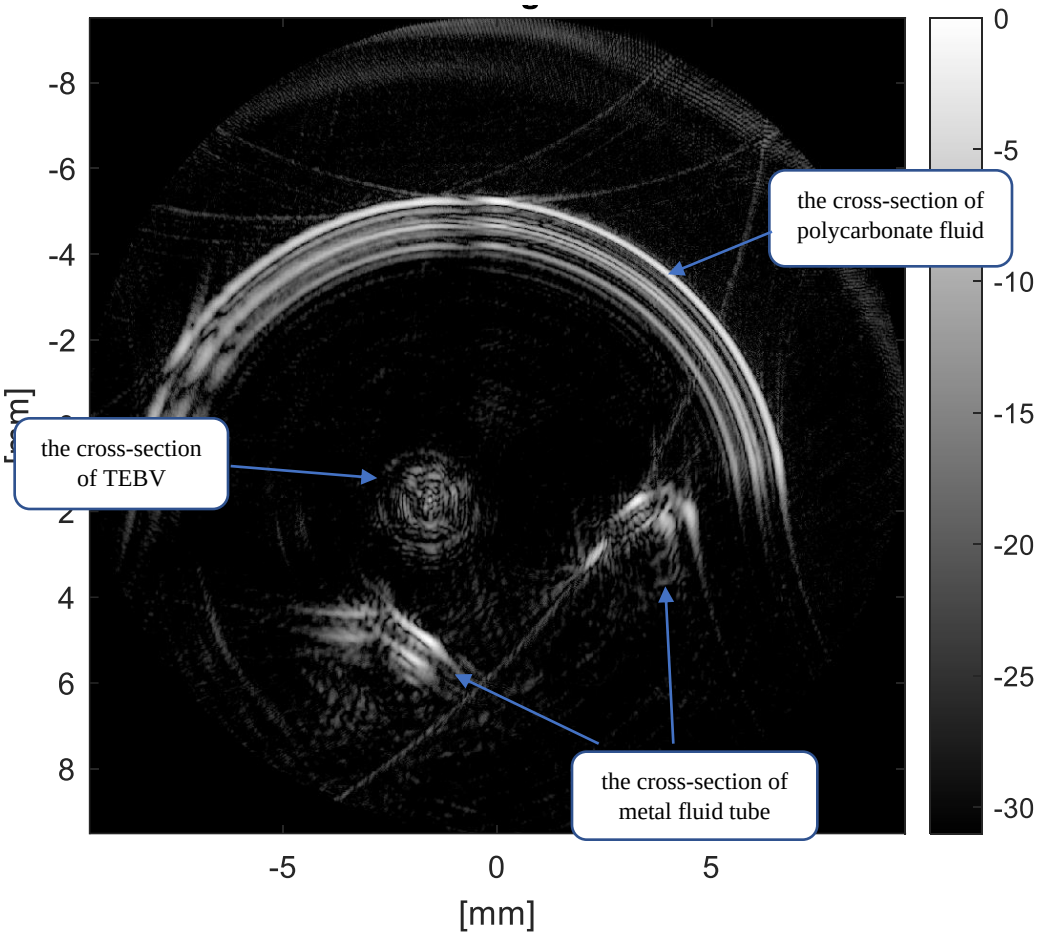

Figure 34. The acquired B-mode image of the partial data algorithm. The data used to acquire this image are from 0° –180° and 540° –720°.

From the acquired image, we have only half of the polycarbonate tube of the bioreactor. However, we can see both the inside and outside diameter of the TEBV.

4. Experiments

To perform imaging, the USCT needs to be prepared, and there are six steps to follow:

- First, set the device to the home position (position the water container actuator at zero degrees).
- Second, fill the water container with water. (Note that the water should be bubbles free).
- Third, position the phantom/bioreactor on the bioreactor holder and fix it with screws to be ridged and parallel to the US transducer.
- Fourth, open the MATLAB data acquisition algorithm (DAQ) and connect the Arduino microcontroller and the US-Key (portable Ultrasound analog-digital converter) USB cable. Set the communication port and speed on the algorithm.
- Fifth, Connect the power supply (24 volts 5-ampere) to the device. When the power supply is connected to the outlet, the indicator light on the GRBL turns on, and the stepper motors start to vibrate. This means that the system is on and ready to perform the image.
- Sixth set the imaging parameter on the DAQ algorithm. The imaging parameters are the step size of angular motion in degrees (number of positions), the number of average data you need from each position, and the name of the 2D matrix file that the data will be stored. (Note. The parameters are changed based on the used sample).

The algorithm will provide 2D unprocessed phantom/bioreactor imaging data when the imaging is done.

4.1 Phantom Experiments

We used a fantom needle experiment to evaluate the point spread function (PSF). PSF describes the response of an imaging system to a point source. We used a needle phantom to evaluate it. Next, we perform imaging on the needle phantom with different diameters and compare the result with another measuring instrument (caliper). The goal is to check the measurement accuracy of the device. (Will the device give the same result if we use the same image parameters but a different size needle?) Next, we continue validation by simultaneously Imaging two needles with different diameters. The goal is not to measure the diameter of both needles but the distance from each other. (It is like simulating the bioreactor). To verify the measurement, we measure the distance between two needles with the caliper and compare it with the measurement from the plot.

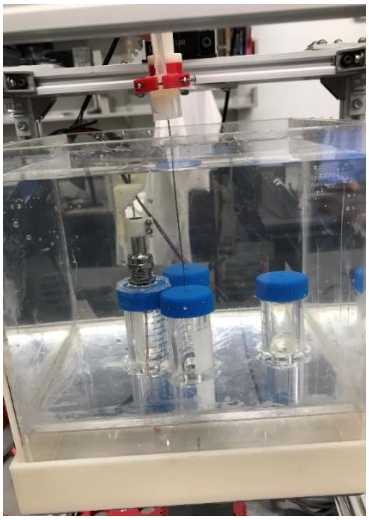

Figure 35. The USCT device imaging needle phantom.

4.2 Experiments, Imaging TEBV

After we validated the system through phantom experiments and assured that the device performed the correct measurement, we continued to image TEBV inside the bioreactor. We performed an Imaging of two TEBV inside a bioreactor labeled the fixed TEBV and new fabricated TEBV. Both TEBVs were fixed. The fixed TEBV was placed on water inside the bioreactor, and the new fabricated TEBV was placed on BPS inside the bioreactor. The goal is to measure the inner-outer diameter and calculate the tissue wall thickness. While performing imaging, we used a laser level with a self-leveling instrument to position the US transducer on the target section in the TEBV shown in figure 36. a) and b). Then, we perform histology on both TEBV and measure the wall thickness with a microscope to verify the measurement.

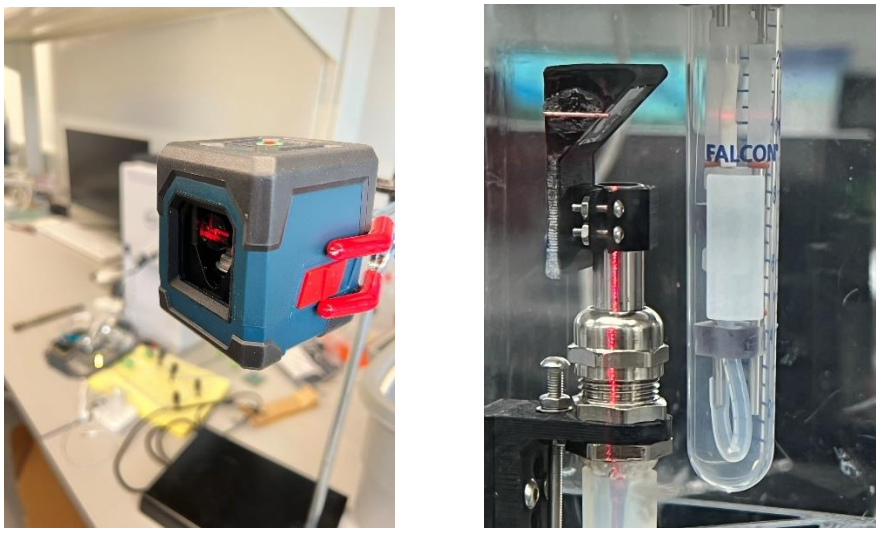

a) b)

Figure 36. a) The laser level with self-leveling, vertical and horizontal line, rotatable 360 degrees. b) The laser guide position of the desired section of the TEBV inside the bioreactor to the US transducer focal point.

4.3 Experiments, effects of intra-bioreactor fluid

The last validation of our system is the TEBV fluid validation. As explained in the introduction, fabrication of TEBV is a complex process, and it needs special conditions (incubator), a source of energy (carbohydrate source), and oxygen for tissue growth. Depending on the state growth of the TEBV, there are different fluids inside the bioreactor. There are three common fluids used on fixed TEBV inside the bioreactor, PBS, DMEM, and water. On the other hand, on the live TEBV, only DMEM fluid is used during growth (water and PBS kills the cell by the osmotic shock). The goal is to find which fluid is better to use on the bioreactor when performing imaging on the fixed TEBV. Because the speed of sound is altered by the density and elasticity of the medium through which it is traveling. In other words, different fluids (PBS, DMEM, and water) have different sound speeds, and it will affect the imaging quality of the TEBV. We image the TEBVs in all three fluids (PBS, DMEM, water) and calculate each fluid's signal-noise ratio (SNR) shown in figures 37 - 39. Statistically, the fluid with the high number is the best fluid to use for the image of the TEBV.

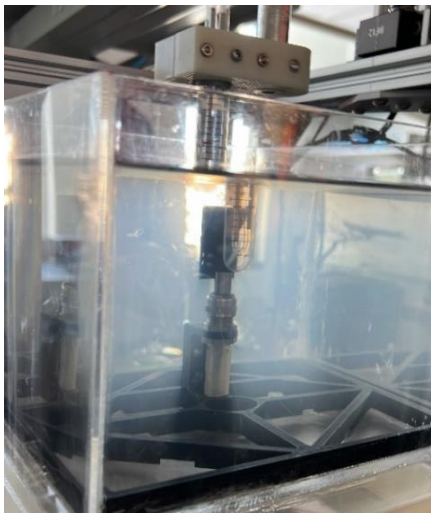

Figure 37. The bioreactor with new TEBV inside filled with water positioned for imaging.

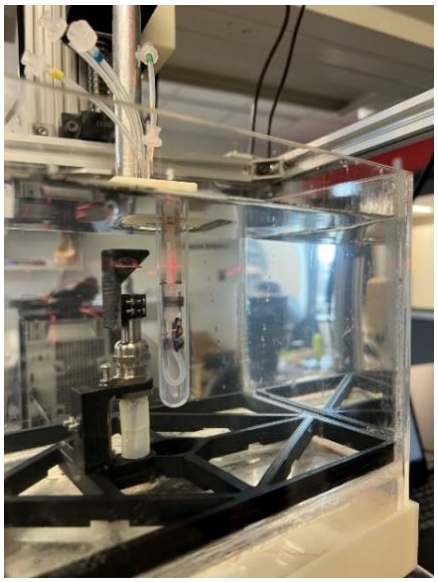

Figure 38. The bioreactor with new TEBV inside filled with PBS positioned for imaging.

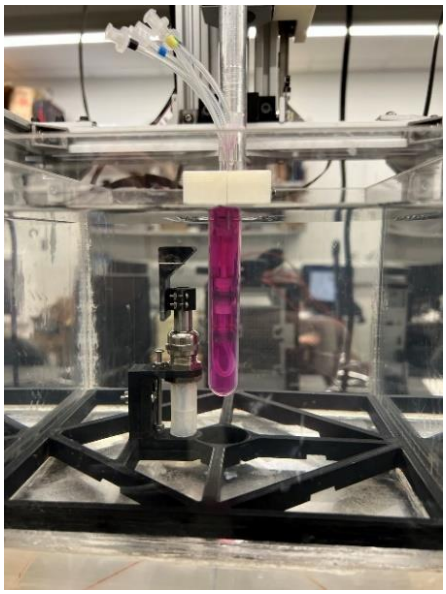

Figure 39. The bioreactor with new TEBV inside filled with DMEM positioned for imaging.

4.4 Histology of TEBV

We perform histology on both the fixed TEBV and the new fabricated TEBV. The TEBVs were processed in the VIP tissue processor, embedded in paraffin, and then sectioned at 5 um. The fixed TEBV was cut in half and embedded both longitudinally and axially, while the new fabricated TEBV was embedded axially only. Tissue sections were then stained for hematoxylin (blue; labels nuclei) and eosin (pink; labels extracellular matrix). Images were then acquired using the Keyence microscope at 4x and 20x magnification. The sections appeared a bit mangled and disorganized because the TEBVs were processed without the supporting tube in the lumen; thus, the tissue processing may have crushed TEBVs.

5. Results

The back-projection algorithm (explained in chapter 3) reconstructs the image from acquired A-lines. The goal is to get the B-mode image of each of the samples/TEBV scanned during the experiments.

There are three steps to follow to acquire the B- mode image from the back-projection algorithm:

- First, open the image reconstruction algorithm on MATLAB and load the data (you need to provide the address of the folder and the name of the matrix that you want to reconstruct).
- Second, set the reconstruction parameter, speed of sound (c), the radius (r), the step size, and the aperture growth (number of the A-line included).
- Third, run the algorithm. The first B-mode image will tell the rough reconstructed image of the sample. Sometimes it may need to tune the parameters like the speed of sound (c), the radius (r), and the aperture growth (numbers of A-line included). After the B-mode is acquired and tuned, the image is ready to measure.

5.1 Phantom evaluation

We used a paper clipper with a 1mm diameter as a needle fantom and performed imaging as described in section 4.1 to evaluate the PSF (the concept is shown in figure 40). The resulting image will describe the imaging system's response to a point source.

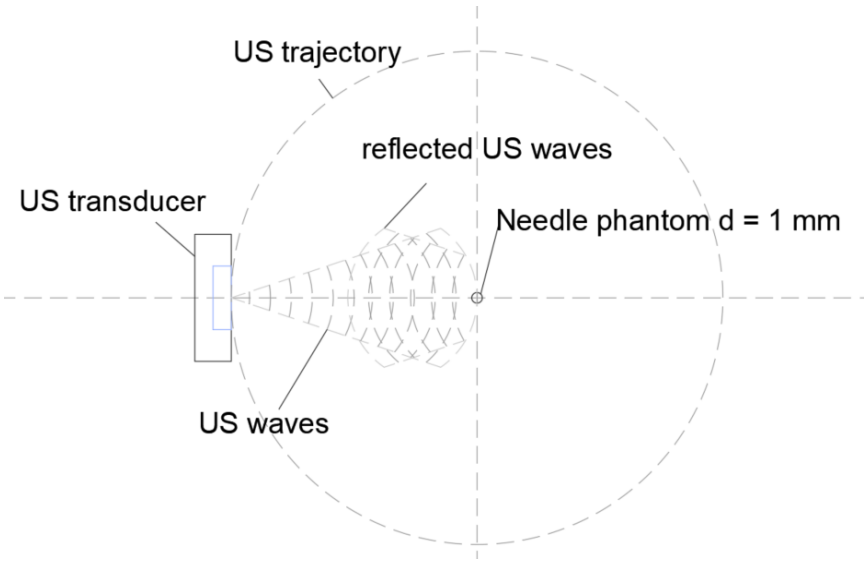

Figure 40. 2D concept of different point targets.

Next, we imaged a different needled fantom to measure the diameter from the plot. (The concept is shown in figure 41). The diameter measured from the plot will be compared with the value of the diameter measured from the caliper. The result will show the accuracy of the measurement and the error. Last we image both needles simultaneously to measure the distance from each other.

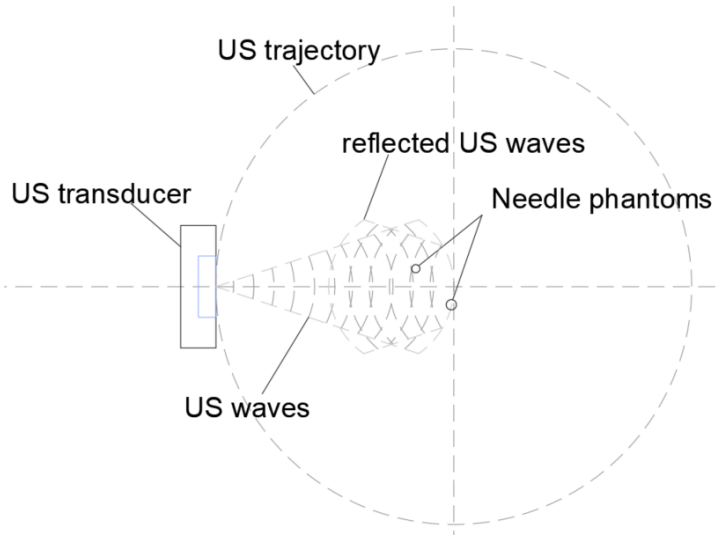

Figure 41. 2D concept of the imaging two needles simultaneously.

The results of the reconstructed image from the point target experiment are shown in figure 42. The acquired B-mode image shows the cross-section of the needle fantom. The reconstruction parameters for the acquired image are the number of samples = 360, number of A-lines included = 120, and speed of sound = 1430. The image looks clear and shows a good shape of the cross-section of the metal needle. From the acquired image, we can measure the diameter of the needle on the plot.

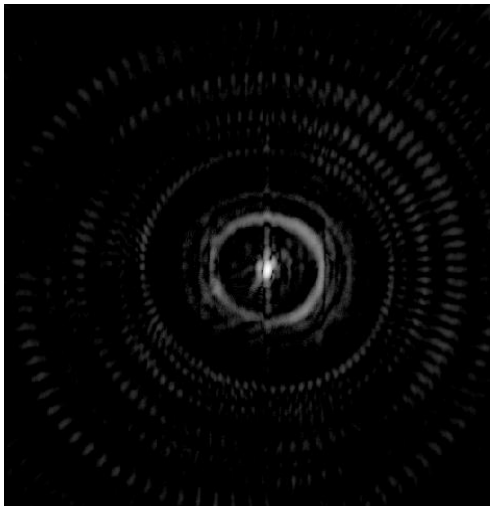

Figure 42. The B-mode image of a point target.

We performed measurements on the acquired B-mode image for all the needle fantom used. From each of the cross-sections of the needle phantom, we took three measurements of the diameter. Next, we performed the arithmetic mean of the three measurements. To compare the result with the verified instrument, we took three measurements of the needle fantom with the caliper. Then we took the mean of the three measurements. The goal is to verify the measurement from the plot with the measurement from the caliper. The result will tell us the accuracy and the error of the device's measurements—figures 43 to 45 show how the measurements are taken from the plot and the caliper.

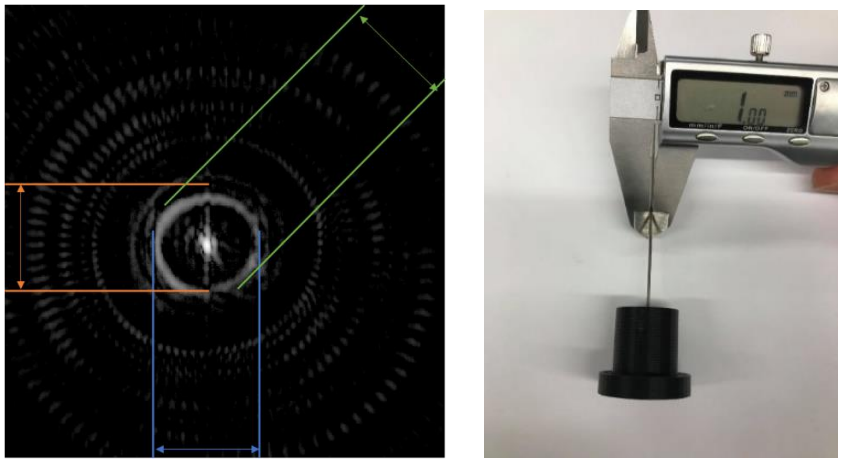

Figure 43. The how the diameter of the needle phantom was measured from the plot = 1.0 mm and from the caliper = 1.0 mm.

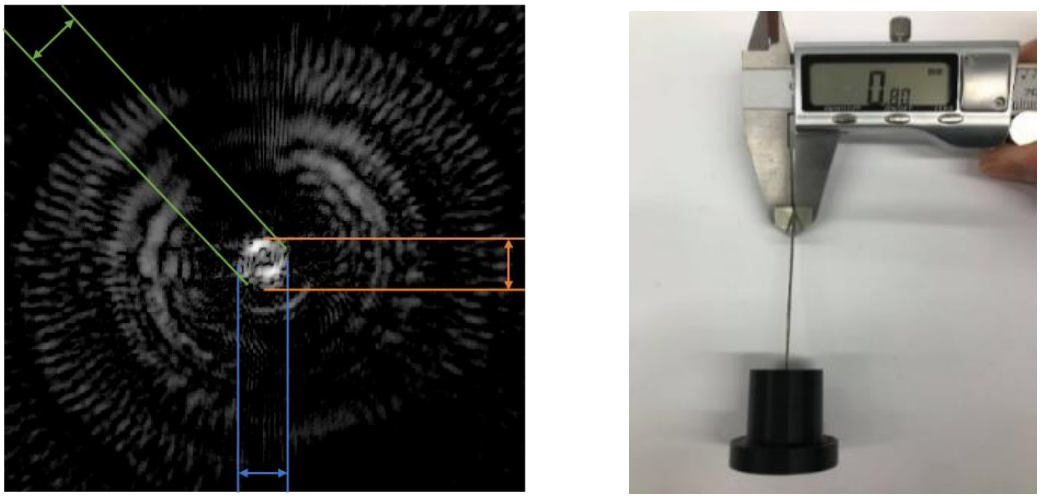

Figure 44. How the diameter of the needle phantom was measured from the plot = 0. 8 mm and from caliper = 0. 8 mm. The image shows a good shape of the cross-section of the metal needle and a low level of noise. The noise reduces the image quality, but we can measure the diameter of the needle on the plot.

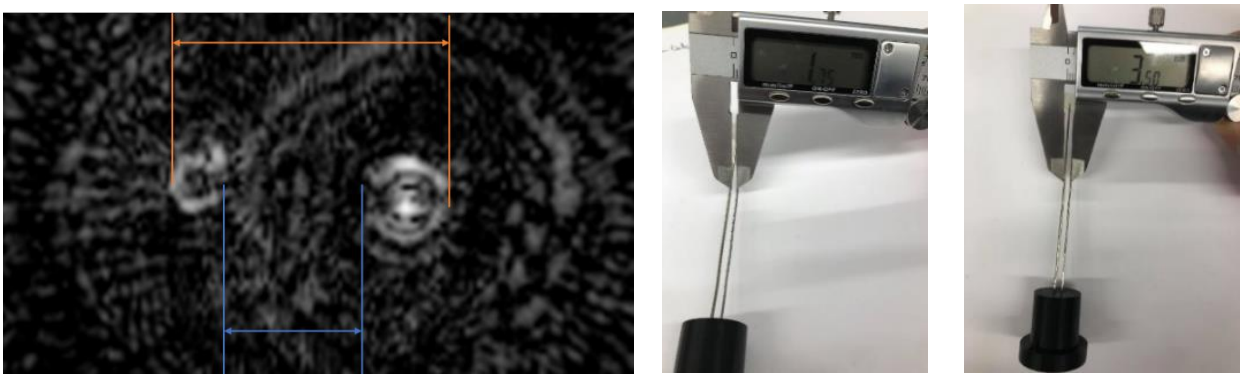

Figure 45. How both fantoms' inside distance (id) and outside distance (od) were measured from the plot and caliper. There is a low level of noise and some artifacts in the acquired image. However, we can see both needles' cross-sections and perform measurements.

Example measurement calculation

id from the plot is |-2.55 – (– 0.8) | = 1.75.

od form the plot is |-3.3 - 0.2| = 3.5.

id form the caliper = 1. 75 mm.

od form the caliper = 3. 5 mm.

Table 2. The plot, the phantom measurement results, the measurement error of the device, and the coefficient of variation.

USCT image validation								
Measurement # (mm)	**Needle phantom measure from a plot**				**Needle phantom measure from the caliper**			
	Needle phantom one measure from the plot	Needle phantom two-measure from the plot	Both needles simultaneously inside measure from the plot	Both needles simultaneously outside measure from the plot	Needle one measure from the caliper	Needle two-measure from the caliper	Both needles simultaneously inside measure from the caliper	Both needles simultaneously outside measure from the caliper
1	0.90	0.74	1.58	3.82	1.000	0.800	1.76	3.51
2	1.20	0.80	1.82	3.43	1.050	0.820	1.74	3.48
3	1.10	0.90	1.86	3.30	0.990	0.780	1.75	3.52
Mean (mm)	**1.067**	**0.813**	**1.753**	**3.517**	**1.013**	**0.800**	**1.750**	**3.503**
Standard deviation	0.153	0.081	0.151	0.271	0.032	0.020	0.010	0.021
Measurement error	**0.053**	**0.013**	**0.003**	**0.013**				
Coefficient of Variation %CV	14.34	9.96	8.61	7.71	3.16	2.50	0.57	0.599

Table 2 shows the experiments result of the phantom needle measure from the plot and caliper. It shows the values of the three measurements taken in different positions for each scanned section. In addition, it shows the calculated arithmetic mean of the measurements, the standard deviation, and the coefficient of variation to show the measurement precision (in %) of the device. Last, the table shows the measurement accuracy of the device, calculated as measurement error = the measurement from the plot (USCT) - the measurement from caliber. The value shows how far from the real value is the measurement done from the USCT.

5.2 TEBV evaluation

The purpose of the USCT device is to perform geometric measurements (the inside and outside diameter) of the TEBV and calculate the wall thickness. After we validated the system, we performed imaging on two TEBVs labeled the fixed TEBV and new fabricated TEBVs. First, we filled the device container with water and placed the bioreactor parallel to the US transducer, as shown in section 4. Next, we directed the US focal point to the section of the TEBV that we wanted to image. The acquired B- mode image will show the cross-section of a particular section of TEBV shown in figure 46. The goal is to measure the inner-outer diameter and calculate the tissue wall thickness. Finally, the TEBV was processed for histology and hematoxylin and eosin (H&E) staining to measure TEBV Wth. Three measurements were taken with a microscope to verify the measurement.

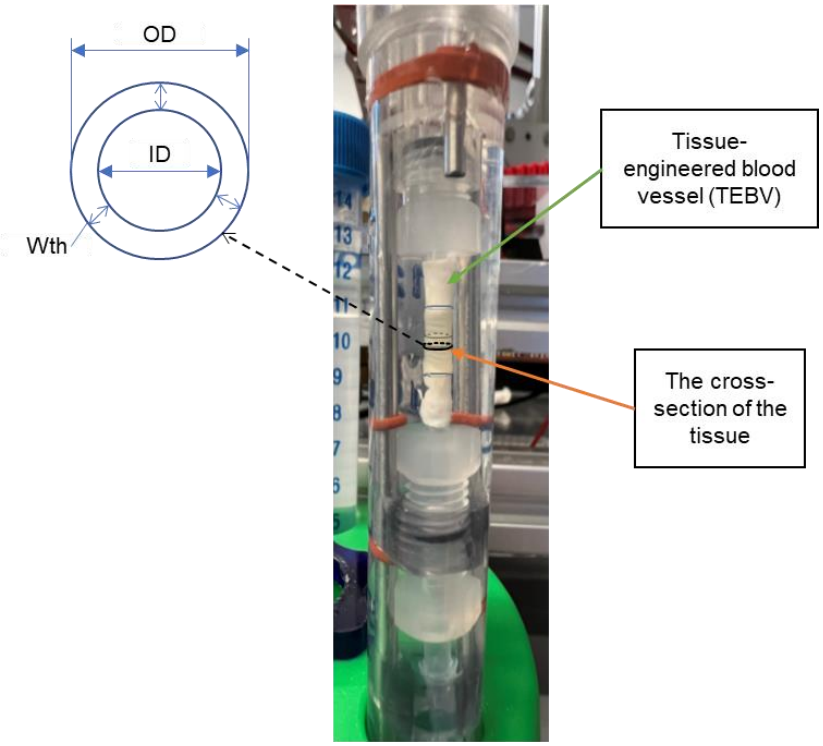

Figure 46. The TEBV inside the bioreactor. Furthermore, it shows the cross-section of the TEBV and how the measurement of ID, OD, and Wth is applied.

The result of the reconstructed image of the fixed TEBV inside the bioreactor experiments is shown in figure 47. The acquired B-mode image shows the cross-section of the fixed TEBV inside the bioreactor. The reconstruction parameters for the acquired image are the number of samples = 720, number of A-lines included = 640, radius = 18.9 mm, and speed of sound = 1430. The image shows a good shape of the cross-section of the fixed TEBV inside the bioreactor (we can see both circles). From the acquired image, we can perform measurements of the ID OD and calculate the Wth of the fixed TEBV from the plot.

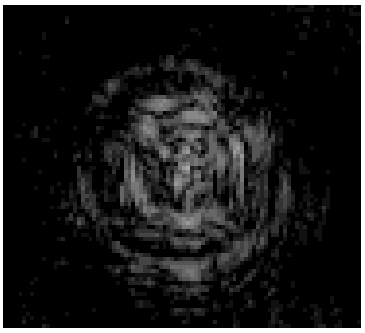

Figure 47. The result of the acquired B-mode of the fixed TEBV inside the bioreactor.

We acquired a B-mode image with the same image parameter that shows the cross-section of the new fabricated TEBV inside the bioreactor shown in figure 48. The image is noisy, but we can see the cross-section of the new fabricated TEBV and perform measurements of the inside and outside diameter on the plot.

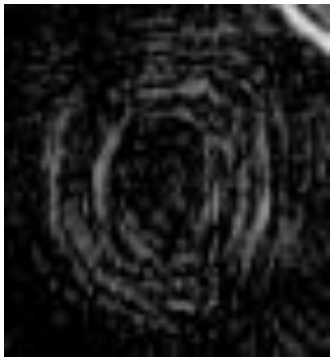

Figure 48. The B-mode image of the new fabricated TEBV inside the bioreactor.

From the acquired B-mode image, we were able to perform geometric measurements on both TEBVs. We used the same process for the TEBV geometric measurement as we did in the phantom needle measurement. First, we took three measurements of the inner and outer diameter of the cross-section TEBV and calculated the wall thickness measurement (shown in figure 49). Next, we took the mean of the three calculated wall thickness measurements. To validate the measurement of the TEBV wall thickness, we performed histology on the TEBV and measured wall thickness from the microscope. We took three measurements of the wall thickness on the cross-section of the TEBV. Then we took the mean of the three measurements.

Figures 49 to 52 show how the measuring process was done on the plot and histology. Table 3 shows the plot and the histology measurement results. In addition, it shows the calculated wall thickness from the plot and the measured wall thickness from histology. Last it shows the measurement error of the device.

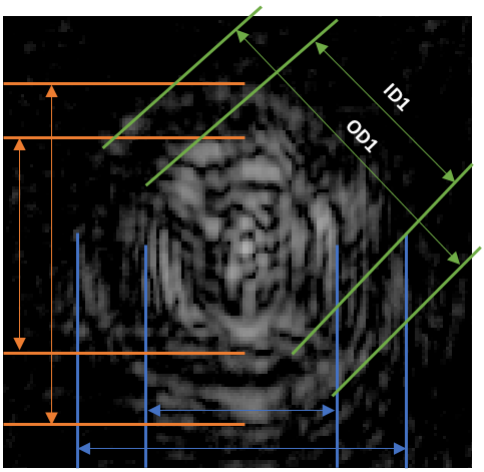

Figure 49. How the inside (ID) and outside diameter (OD) of the fixed TEBV. Furthermore, it shows where the measurements are taken from the plot (the colored arrows in the image).

Example measurement calculation

OD1 = (3.0 -0.4) = 2.6mm

ID1 = 2.6 – 1.15 = 1.35mm

The TEBV thickness 1 = 2.6 – 1.35 = 1.25 /2 = 0.625mm

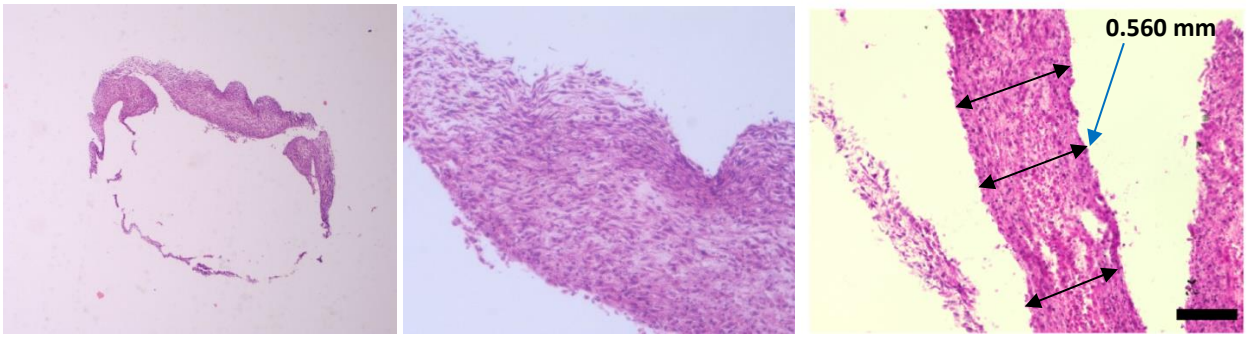

a) b) c)

Figure 50. The fixed TEBV was measured from the microscope a) at 4x. Scale = 0.1 mm, b) the wall of the fixed TEBV at 20x. c) Sample measurement acquisition of the fixed TEBV at 20x. Scale = 0.2 mm.

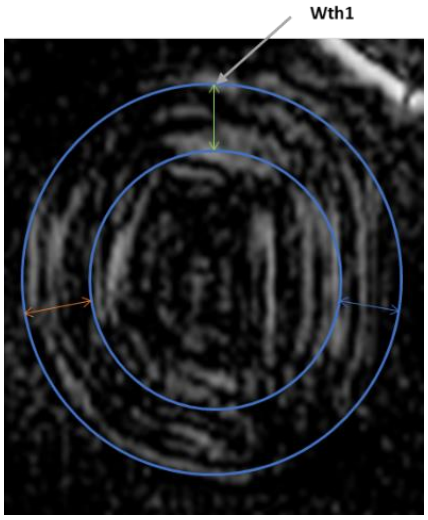

Figure 51. The cross-section of the new fabricated TEBV with highlighted the inside (ID) and outside diameter (OD). Furthermore, it shows where the measurements are taken from the plot (the colored arrows in the image).

Example measurement calculation

OD1 = (3.45-1.4) = 1.99

ID1= 1.1mm

The TEBV thickness 1 = 1.99 – 1.1 = 0.89 /2 = 0.445mm

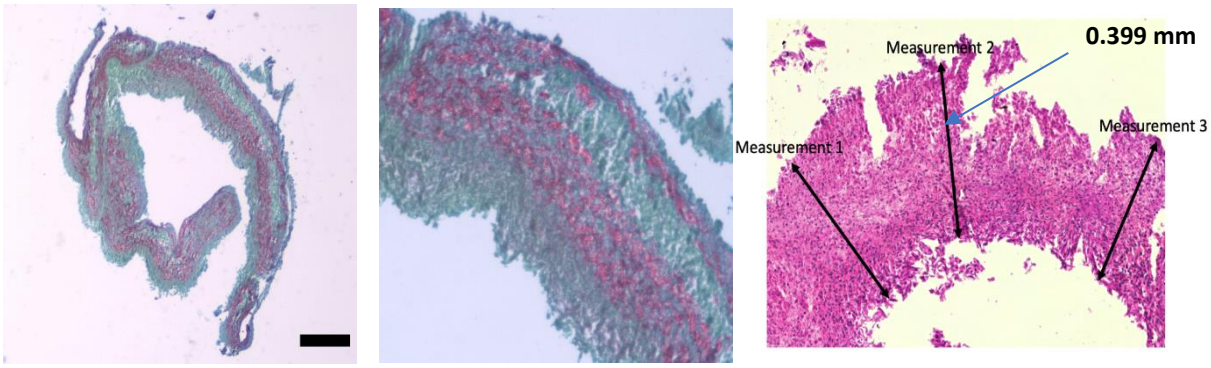

a) b) c)

Figure 52. The new fabricated TEBV was measured from the microscope a) at 4x. Scale =250 um, b) the wall of the new fabricated TEBV at 20x. c) Sample measurement acquisition of the fixed TEBV at 20x. Scale = 0.2 mm.

Table 3. The TEBV measurement results of the plot and the histology. It shows the calculated wall thickness, the standard deviation, and the coefficient of variation measured from the plot and histology.

	TEBV Wall Thickness Analyses						
Measurement # (mm)	**TEBV one**					**TEBV two**	
	Histology			**USCT**	**USCT**	**Histology**	**USCT**
	new TEBV on PBS sec 1	**new TEBV on PBS sec 2**	**new TEBV on PBS sec 3**	**the plot of the new TEBV**	**the plot of the new TEBV sec 2**	**fixed TEBV on water circ**	**the plot of the fixed TEBV**
1	0.319	0.323	0.389	0.440	0.430	0.618	0.625
2	0.290	0.457	0.373	0.476	0.480	0.587	0.634
3	0.441	0.417	0.324	0.420	0.460	0.476	0.617
Mean (mm)	**0.350**	**0.399**	**0.362**	**0.445**	0.457	**0.560**	**0.625**
Standard deviation	0.08	0.069	0.034	0.028	0.025	0.074	0.0085
Measurement error (mm)	0.095	0.046	0.083			0.065	
Coefficient of Variation %CV	22.86	17.29	9.39	6.29	5.47	13.21	1.36

Table 3 shows the experiments result of the TEBV wall thickness measurements from the plot and histology. It shows the values of the three measurements taken in different positions for each scanned section. In addition, it shows the calculated arithmetic mean of the measurements, the standard deviation, and the coefficient of variation to show the measurement precision (in %) of the device. Last, the table shows the measurement accuracy of the device, calculated as measurement error = the measurement from the plot (USCT) - the measurement from histology. The value shows how far from the real value is the measurement done from the USCT.

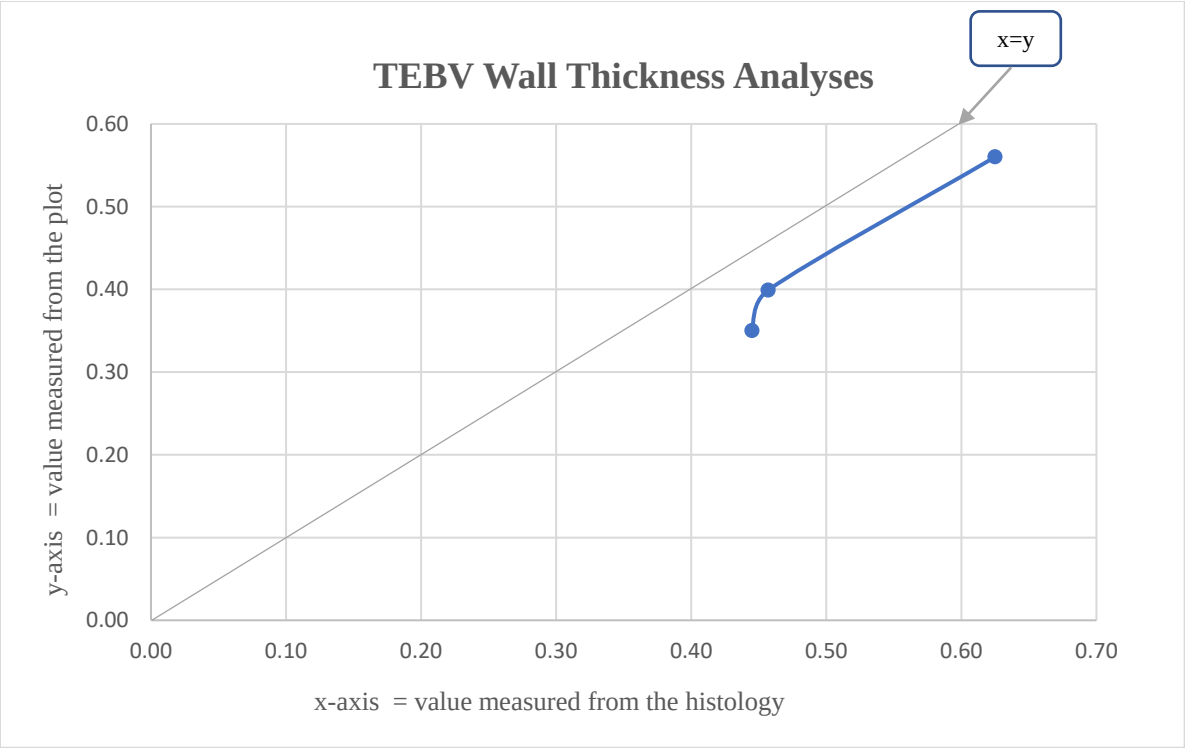

Graph 1. TEBV wall thickness measurement data with the TEBV wall thickness measurements from the histology. From the graph, we can see that the measurements are almost linear.

5.3 Effects of intra-bioreactor fluid

One of the factors that can attenuate the US signal and impact the image quality is the fluid inside the bioreactor. Therefore, the last validation of our system is the TEBV solution validation. The goal is to find which solution is better to use on the bioreactor when performing imaging. We did three different experiments with the same TEBV, but we filled the bioreactor with PBS, DMEM, and water and then performed imaging. We used the same imaging parameters for all three fluids: the number of samples = 720, the number of A-lines included = 640, radius = 19 mm, and speed of sound = 1410. To evaluate which solution is better to use, we calculate each solution's signal-noise ratio (SNR) and compare it. The solution with the high number is the best solution to use for image TEBV. The resulting B-mode image of the new fabricated TEBV inside the bioreactor is shown in figure 53. The images are noisy and have some artifacts. Nevertheless, we can see the cross-section of the TEBV on the three used fluids and perform geometric measurements of the inside and outside diameter on the plot. We can notice that the acquired image from water and PBS solution looks closely the same because they have approximately the same speed of sound. To select which solution is better, we need to calculate the SNR.

a) b) c)

Figure 53. The B-mode image of the bioreactor with a new fabricated TEBV inside filled with a) water, b) PBS, c) DMEM.

The SNR (in dB) compares the desired signal level to the background noise level. We calculate the signal-noise – ratio (SNR) from MATLAB by selecting the region of interest and the background in the image. Figures 45 and 55 show the region's interest (in blue), and the background (in green) used to calculate the SNR. Table 4. shows measurement results of the new fabricated TEBV imaged on different fluids and the SNR of the image.

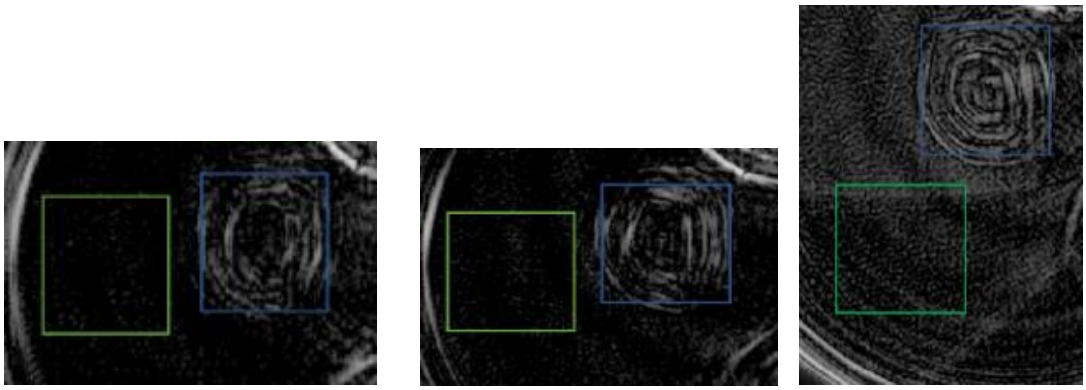

Figure 54. Selected area for calculating SNR of new fabricated TEBV on water, PBS, and MDEM (the region of interest is highlighted with blue, and the background region is highlighted with green)

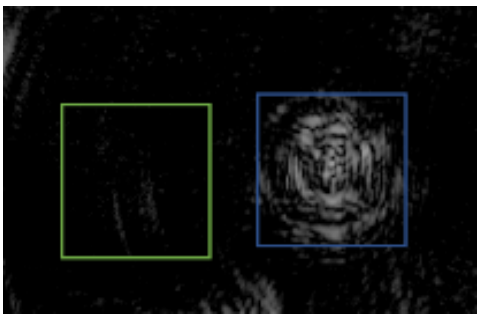

Figure 55. Selected area for calculating SNR of the fixed TEBV on water.

Table 4. Measurement results of the new fabricated TEBV imaged on different fluids and the SNR of the image.

Effects of intra-bioreactor fluid analysis						
Measurement # (mm)	**New fabricated TEBV Imaged in different fluids**					
	TEBV on Water	**TEBV on PBS**	**TEBV on DMEM**	**Histology of new TEBV**	**The fixed TEBV on water**	**Histology Of the fixed TEBV**
1	0.450	0.440	0.525	0.323	0.625	0.618
2	0.481	0.476	0.534	0.457	0.634	0.587
3	0.432	0.420	0.517	0.417	0.617	0.476
Mean (mm)	**0.454**	**0.445**	**0.525**	**0.399**	**0.625**	**0.560**
Standard deviation	0.025	0.028	0.009	0.069	0.0085	0.074
Measurement error (mm)	0.055	0.046	0.126			
SNR	**25.36**	**18.01**	**12.83**		**27.05**	
Coefficient of Variation %CV	5.507	6.292	1.714	17.293	1.360	13.214

Table 4 shows the experiments result of the effects of intra-bioreactor fluid. In addition, it shows the calculated value of the SNR of each fluid (MDEM, PBS, water) used in the bioreactor when performing imaging of the new TEBV. From the table, we can say that Water and PBS are the best fluid for performing imaging of the fixed TEBV inside the bioreactor. However, even though MEDM shows a low level of SNR and the resulting image has a high level of noise, we still can measure the inner-outer diameter and calculate the wall thickness from the cross-section of the TEVB shown in figure 53. c).

6. Discussion

We build an ultrasound computer tomography (USCT) imaging system to monitor tissue-engineered blood vessels (TEBV). The USCT system consists of a single-element transducer that moves in a circular trajectory along the bioreactor and collects A-lines of the cross-section of the TEBV. A back-projection algorithm was used to reconstruct the image from acquired A-lines. Experiments were conducted to validate the imaging system and a needle phantom to evaluate the point spread function (PSF).

The phantom experiments demonstrate the capability of the USCT device to perform imaging on nonhomogenous targets. System stability and repeatability to perform imaging on the desired target are tested on the hardware. The ultrasound imaging collected by the platform proves the hardware design. And the acquired images before reconstruction suggest that the proposed tomography device provides enough precision in motion to perform imaging at TEBV. To sensor S1 (shown in figure 22), create a close loop control of the actuator to minimize the positioning error. This result proves the feasibility of the ultrasound computer tomography device that can imagine nonhomogeneous media. With a deflection of 0.03 mm of the mechanical rotation shaft, a step size of 0.5°, and a maximum of 720 sample positions. The device can perform imaging of TEBV. Even though the current US transducer gives low image spatial resolution (around 0.3 mm), it still provides high contrast B-mode images to perform geometric measurements.

After the system was validated, TEBV was imaged. Histology was used to validate the dimensions of the TEBV obtained from the image. From the scanned image, we could successfully visualize the cross-section of the TEBV. In addition, from the cross-section of the TEBV, we could perform geometric measurements (inner diameter (ID), the outer diameter (OD)) and calculate the wall thickness (Wth) shown in figure 49. To verify the measurements and compare the results, the TEBV was processed for histology and hematoxylin and eosin (H&E) staining to measure TEBV wall thickness. The experiment results showed that the USCT imaging system could provide geometric data of the TEBV without damaging the tissue.

However, to simplify and reduce the measurement error of the device, the image quality needs to be improved. The acquired images do not have high contrast to background signals. Several factors limit the USCT image quality. The polycarbonate tube of the bioreactor attenuates the US signal before reaching the TEBV, and the fluids used inside the bioreactor have different speeds of sound compared to water shown in table 4. Furthermore, we used the most straightforward reconstruction method, and the device's US transducer has a low central frequency (6MHz). In future work, we improve the reconstruction algorithm for better image quality, perform imaging with live-cell TEBV, and extend the device's capacity to calculate fluid's doppler effect inside the bioreactor.

On the system implementation level, the construction of the USCT costs 2700 USD. The construction costs are included the aluminum frame, the PVC water container, the stepper motors actuators, the manufactured flanged bearing the 3D printed support, the Arduino microcontroller with the GRBL shield, and the US transducer with the US-key digitizer. The PC costs can be ignored. The experiment successfully proves that the low-cost device can perform tomography imaging.

However, there are some limitations when the USCT device performs imaging. The device needs calibration before imaging, and it needs to start imaging at the home position (if not, the image will not be good). The water container needs to be cleaned before and after imaging the new TEBV. The device can perform no more than 4 hours of imaging because the portable US-Key (DAQ) overheats and attenuates the US signal.

When the device performs phantom imaging, the image parameters are the step size = 1, the number of positions = 360, the number of averaging = 10, and the total scanning time = 8 min. As a result, the image shows a good shape of the low cross-section level of noise, and we can measure the diameter shown in figure 42. However, this is different when we perform TEBV imaging. When we perform TEBV imaging, the imaging parameters combine the scanning time and the image resolution. As a result, the image parameters are higher than the phantom imaging parameter, the step size = 0.5, the number of positions = 720, the number of averaging = 10, and the total scanning time = 28 min. As a result, the acquired B-mode images have a low noise level, but we can see the shape of the cross-section of the TEBV and perform measurements of the ID OD and calculate the Wth shown in figures 47-48.

Both scanning time and resolution are essential parameters when performing TEBV imaging because we want to have a high resolution of the B – mode image without exaggerating the scanning time, no more than 35 minutes. Furthermore, the scanning time relates to the time the live TEBV can resist out of the incubator without damaging the tissue. Therefore, based on our experiment, we conclude that 28 minutes is necessary for the USCT device to perform imaging of the TEBV.

On the other hand, image reconstruction requires low computational power. The quantification below is measured at the standard-configured PC (CPU: I9 intel 8-core processor, Memory: 16 Gb, GPU: Nvidia GTX 1660 Ti). With the data size of 15000 samples in each A-line, Delay- and-Sum (DAS) reconstruction takes about 10 - 20 minutes to reconstruct the B-mode image (But with better computational power, it takes less reconstruction time). The reconstruction of parameters for acquiring the B-mode image of TEBV is the number of samples = 720, the numbers of A-line included = 640 r= 18 – 20 mm, the speed of sound = 1410 -1430. An optimized reconstruction algorithm or parameters that generate similar image quality can be investigated for future research.

Last, the results demonstrated that the USCT device could image and perform measurements of the inner diameter (ID) and the outer diameter (OD) and calculate the wall thickness (Wth) of the TEBV inside the bioreactor. Hence the USCT imaging system could be an evaluating tool to provide serial, non-destructive geometry measurements of the TEBV during culture.

7. Conclusion

This research introduces and tests a low-cost open-source ultrasound computer tomography (USCT) imaging system that provides an alternative way to achieve non-invasive TEBV growth monitoring. The device combines hardware and software to perform imaging of the TEBV inside the bioreactor 360 degrees on all its lengths and record the tissue changes over time.

The research answers the question of developing a new non-destructive evaluation tool to perform serial geometry measurements of the TEBV to monitor tissue development and remodeling. The unique characteristic of the USCT device is that the device is designed specifically to monitor TEBV and the aluminum manufacturer frame and gives the system stability and repeatability in motion control. Additionally, by adding the z-axis actuator, the USCT device can be converted into a 3D computer tomography device and extend its use.

This research also investigates the use of the device to perform geometric measurements of the TEBV and the effects of intra-bioreactor fluid use on the bioreactor when performing imaging on the fixed TEBV. The device is used to get the cross-section of the TEBV and perform geometric parameters of the TEBV (inner diameter (ID) and outer diameter (OD)) and calculate the wall thickness (Wth). Furthermore, the speed of sound is affected by the density and elasticity of the medium through which it is traveling. Therefore, finding which fluid (PBS, DMEM, water) is better to use when performing imaging of the TEBV inside the bioreactor.

Last, the study demonstrates that the USCT imaging system fulfills the goal of providing serial, non-destructive geometry measurements of the TEBV during culture. Water and PBS are the best fluid for performing imaging of the fixed TEBV inside the bioreactor. However, MEDM shows a low SNR level, but we can still measure the inner-outer diameter and calculate the wall thickness from the cross-section of the TEVB shown in figure 53. c).

8. References

[1] Laura Teodori, Annunziata Crupi, Alessandra Costa, Alberto Diaspro, Susanne Melzer, Attila Tarnok, Three-dimensional imaging technologies: a priority for the advancement of tissue engineering and a challenge for the imaging community, Journal of Biophotonics Volume 10, Issue 1 p. 24-45, Apr 25, 2016, (doi.org/10.1002/jbio.201600049)

[2] H.GemmekeN.V.Ruiter, Three-dimensional imaging technologies: 3D ultrasound computer tomography for medical imaging, Nuclear Instruments, and Methods in Physics Research Section A: Accelerators, Spectrometers, Detectors and Associated Equipment Volume 580, Issue 2, Oct 1, 2007, Pages 1057-1065, https://doi.org/10.1016/j.nima.2007.06.116)

[3] Hannah A. Strobel, Ph.D.,1, * Tracy A. Hookway, Ph.D., 1,2,3, * Marco Piola, Ph.D.,4 Gianfranco Beniamino Fiore, Ph.D.,4 Monica Soncini, Ph.D.,4 Eben Alsberg, Ph.D.,5,6 and Marsha W. Rolle, PhD1, Assembly of Tissue-Engineered Blood Vessels with Spatially Controlled Heterogeneities, Tissue Eng Part A, 24(19-20):1492-1503 (2018). DOI: 10.1089/ten.tea.2017.0492

[4] Gemmeke, H., Ruiter, N. V., "3D ultrasound computer tomography for medical imaging," Nuclear Instruments and Methods in Physics Research Section A: Accelerators, Spectrometers, Detectors, and Associated Equipment, 580(2):1057-1065 (2007).

[5] Stotzka, R., Gemmeke, H., "Medical imaging by ultrasound computer tomography," Proc. SPIE 4687 (2002)

[6] Natterer, F., "A propagation-back-projection method for ultrasound tomography," Inverse Problems 11, 1225-1232 (1995).

[7] Devaney, A. J., "A filtered backpropagation algorithm for diffraction tomography," Ultrasonics Imaging, 4(4):336- 350 (1982).

[8] Paul Kumar Upputuri 1, Kathyayini Sivasubramanian 1, Chong Seow Khoon Mark 1, Manojit Pramanik, Recent developments in vascular imaging techniques in tissue engineering and regenerative medicine, Biomed Res int. 2015; 2015:783983. doi:10.1155/2015/783983

[9] Yu Shrike Zhang1, Junjie Yao2, Imaging Biomaterial–Tissue Interactions, Trends in Biotechnology 36, Issue 4, April 2018, 403-414 doi.org/10.1016/j.tibtech.2017.09.004

[10] S. Wang, I.V. Larina, 8 - High-resolution imaging techniques in tissue engineering, Monitoring, and Evaluation of Biomaterials and their Performance In Vivo 2017, (151-180): https://doi.org/10.1016/B978-0-08-100603-0.00008-0

[11] Binita Shrestha, Frank DeLuna, Mark A. Anastasio, Jing Yong Ye, and Eric M. Brey, Photoacoustic Imaging in Tissue Engineering and Regenerative Medicine, Tissue Engineering Part B: Reviews.Feb2020.79-102 doi.org/10.1089/ten.Feb.2019.0296

[12] Chen, W., Liu, S., Yang, J., Wu, Y., Ma, W., Lin, Z. Nondestructive Monitoring of Degradable Scaffold-Based Tissue-Engineered Blood vessel Development Using Optical Coherence Tomography. J. Vis. Exp. (140), e58040, doi:10.3791/58040 (2018)

[13] Wanwen Chen, 1 Shangmin Liu, 2 Junqing Yang, 1 Yueheng Wu, 2 Wentao Ma, two and Zhanyi Lin 3, Non-destructive monitoring of degradable scaffold-based tissue-engineered blood vessel development using optical coherence tomography," J Vis Exp. 2018; (140): 58040. 2018 Oct 3. (DOI: 10.3791/58040)

[14] Abhijit A Gurjarpadhye 1, Bryce M Whited, Alana Sampson, Guoguang Niu, Kriti Sen Sharma, William C Vogt, Ge Wang, Yong Xu, Shay Soker, Marissa Nichole Rylander, Christopher G Rylander, "Imaging and characterization of bioengineered blood vessels within a bioreactor using free-space and catheter-based OCT," Lasers in Surgery and Medicine 45:391-400 (2013). DOI: 10.1002/lsm.22147.

[15] Gemmeke, H., Ruiter, N. V., "3D ultrasound computer tomography for medical imaging," Nuclear Instruments and Methods in Physics Research Section A: Accelerators, Spectrometers, Detectors, and Associated Equipment, 580(2):1057-1065 (2007).

[16] Schuetzenberger, K., Pfister, M., Messner, A.et al. "Comparison of optical coherence tomography and high-frequency ultrasound imaging in mice for the assessment of skin morphology and intradermal volumes," Sci Rep 9, 13643 (2019).

[17] Fornell, D., "The advantages and disadvantages of OCT vs. IVUS," di. cardiology, May 18, 2011, /www.dicardiology.com/article/advantages-and-disadvantages-oct-vs-ivus

[18] Anne M. Leferink, Clemens A. van Blitterswijk, and Lorenzo Moroni "Methods of Monitoring Cell Fate and Tissue Growth in Three-Dimensional Scaffold-Based Strategies for In Vitro Tissue Engineering," Tissue Engineering Part B: ReviewsVol. 22, No. 4, Mar 1, 2016, doi.org/10.1089/ten.teb.2015.0340

[19] Seung Yun Nam, Laura M. Rickles, Laura J. Suggs, and Stanislav Y. Emelianov," Imaging Strategies for Tissue Engineering Applications" Tissue Engineering Part B: Reviews Vol. 21, No. 1, Aug 18, 2014, doi.org/10.1089/ten.teb.2014.0180

[20] Mohd Taufiq Mohd Khairia Sallehuddin Ibrahima Mohd Amri Md Yunusa Mahdi Faramarzia Goh Pei Sean Jaysuman Pusppanathanc Azwad Abid," Ultrasound computed tomography for material inspection: Principles, design, and applications," Measurement, Volume 146, November 2019, Pages490-523, doi.org/10.1016/j.measurement.2019.06.053

[21] David B. Berry, Erin K. Englund, Shaochen Chen *, Lawrence R. Frank * and Samuel R. Ward," Medical imaging of tissue engineering and regenerative medicine constructs, Biomater. Sci., 2021, 9, 301-314, 6th August 2020, DOI: 10.1039/D0BM00705F

[22] N. Castro, S. Ribeiro, M. M. Fernandes, C. Ribeiro, V. Cardoso, V. Correia, R. Minguez, S. Lanceros-Mendez, Physically Active Bioreactors for Tissue Engineering Applications, advance biosystems Sept 13, 2020, https://doi.org/10.1002/adbi.202000125

[23] Egor Morokov, Elena Khramtsova, Elena Kuevda, Elena Gubareva, Timothei Grigoriev, Ksenia Lukanina, Vadim Levin "Non-invasive ultrasound imaging for assessment of intact microstructure of extracellular matrix in tissue engineering," Artificial Organs Volume43, Issue 11, Jun 13, 2019, doi.org/10.1111/aor.13516

[24] Alyssa A Appel, Mark A Anastasio, Jeffery C Larson, Eric M Brey, Imaging challenges in biomaterials and tissue engineering, Biomaterials, Volume 34, Issue 28, September 2013 Sep;34(28):6615-30 doi.org/10.1016/j.biomaterials.2013.05.03